The Journal of Chemical Physics

RESEARCH ARTICLE | FEBRUARY 08 2021

The Raman jet spectrum of *trans*-formic acid and its deuterated isotopologs: Combining theory and experiment to extend the vibrational database

Special Collection: **Quantum Dynamics with ab Initio Potentials**

Arman Nejad ; Edwin L. Sibert, III

J. Chem. Phys. 154, 064301 (2021)
https://doi.org/10.1063/5.0039237

The Journal of Chemical Physics | ARTICLE | scitation.org/journal/jcp

The Raman jet spectrum of *trans*-formic acid and its deuterated isotopologs: Combining theory and experiment to extend the vibrational database

Cite as: J. Chem. Phys. **154**, 064301 (2021); doi: 10.1063/5.0039237
Submitted: 2 December 2020 • Accepted: 13 January 2021 •
Published Online: 8 February 2021

Arman Nejad[1,a)] and Edwin L. Sibert III[2,b)]

AFFILIATIONS

[1] Institute of Physical Chemistry, Georg August University of Göttingen, Tammannstraße 6, 37077 Göttingen, Germany
[2] Department of Chemistry and Theoretical Chemistry Institute, University of Wisconsin-Madison, Madison, Wisconsin 53706, USA

Note: This paper is part of the JCP Special Topic on Quantum Dynamics with *ab initio* Potentials.
[a)] **Author to whom correspondence should be addressed:** anejad@gwdg.de
[b)] **Electronic mail:** elsibert@wisc.edu

ABSTRACT

Revisiting recently published Raman jet spectra of monomeric formic acid with accurate high order perturbative calculations based on two explicitly correlated coupled-cluster quality potential energy surfaces from the literature, we assign and add 11 new vibrational band centers to the *trans*-HCOOH database and 53 for its three deuterated isotopologs. Profiting from the synergy between accurate calculations and symmetry information from depolarized Raman spectra, we reassign eight literature IR bands up to 4000 cm^{-1}. Experimental detection of highly excited torsional states (ν_9) of *trans*-HCOOH, such as $4\nu_9$ and $\nu_6 + 2\nu_9$, reveals substantial involvement of the C–O stretch ν_6 into the O–H bend/torsion resonance $\nu_5/2\nu_9$, which is part of a larger resonance polyad. Depolarization and isotopic C-D substitution experiments further elucidate the nature of Raman peaks in the vicinity of the O–H stretching fundamental (ν_1), which seem to be members of a large set of interacting states that can be identified and described with a polyad quantum number and that gain intensity via resonance mixing with ν_1.

I. INTRODUCTION

Since its first spectroscopic detection in 1938,[1] the internal dynamics of formic acid have continuously been motivating experimental[2–12] and theoretical[13–18] investigations. The number of experimentally determined (ro-)vibrational parameters of formic acid in its ground and vibrationally excited states is enormous (see Refs. 6–9, 19, and 20 and references therein), the experimental data further extending to its ^{13}C,[21–28] ^{18}O,[3,29,30] and ^{2}H isotopologs.[19,31–37] One of the reasons for this interest results from formic acid having two low-lying conformational isomers, depicted in Fig. 1. They are connected through the large-amplitude O–H torsion, which is responsible for many interesting and challenging dynamical features that we will touch upon in this work. It is well known that this motion is not appropriately treated using rectilinear normal coordinates, as the torsion corresponds to atomic displacements perpendicular to the figure plane in straight line paths. To correctly investigate this degree of freedom and its coupling to the remaining degrees of freedom, one has to treat this motion as a true internal torsional coordinate.[38,39] From the perspective of this paper, the large anharmonicity of the torsion causes this vibration to tune in and out of resonance interactions as it is excited to increasingly high vibrational levels. This tuning provides an opportunity to interrogate a wide range of anharmonic couplings by matching

FIG. 1. Conformational isomers of the formic acid monomer.

theory with experiment. As an example, several experimental[12] and computational[16,17] studies have added clarity to the long-debated question of the assignment of the O–H in-plane bend ν_5 and O–H torsional overtone $2\nu_9$, which are in resonance. The higher IR intensity of the overtone has obscured the assignment of this resonance pair in the past as the more intense band was believed to be the fundamental.[8,40] Recently published Raman jet spectra intuitively support the recent proposal,[40] i.e., to assign the fundamental to 1306 cm^{-1} and the overtone to 1220 cm^{-1}, where the band integral of the fundamental is seven times higher compared to the overtone.

This reassignment was triggered by recent high level anharmonic vibrational calculations, namely, vibrational configuration interaction using an internal coordinate path Hamiltonian (ICPH)[16] and multi-configuration time-dependent Hartree (MCTDH),[17] further providing the community with two full-dimensional CCSD(T)-F12 (explicitly correlated coupled-cluster singles, doubles, and perturbative triples) quality potential energy surfaces of *cis*- and *trans*-formic acid. While the reported MCTDH and ICPH results for *trans*-HCOOH agree well with each other and available experimental reference data, deviations for *cis* are significant with root-mean-square deviations of 14 cm^{-1} and 49 cm^{-1} for one- and two-quantum states, respectively.[16,17] Richter and Carbonnière consulted VPT2 energies for the nine fundamentals using both surfaces to rule out significant contributions from both potentials to the above mentioned discrepancies.[17]

In this work, we use these two surfaces to make detailed comparisons with experiment for several isotopologs of both isomers. Our comparisons will detail the differences in the harmonic and anharmonic contributions, going beyond VPT2 and fundamentals. To solve for the vibrational eigenstates, we use high order canonical Van Vleck perturbation theory (CVPT) as implemented in curvilinear coordinates. We shall see that this approach provides accurate energies, allows us to describe couplings with relatively small matrices, and provides a test of perturbative methods.

To benchmark both potentials, we can build on a wide range of perturbation-free vibrational reference data for *trans*-HCOOH extending far beyond fundamentals, and particularly noteworthy is the enormous list of IR bands reported by Freytes *et al.*[7] Comprehensive Raman spectra of formic acid and its three deuterated isotopologs were published four decades ago by Bertie *et al.*[4,41] As their significant work was concerned with the formic acid dimer, the assignment of non-fundamental monomeric bands from their spectra is impaired by overlapping dimer contributions.[40] Recently published Raman jet spectra, which build on earlier studies,[42] are optimized for monomer signals and as an additional feature of the heatable setup that is used,[43] peaks due to cold monomer, clusters, or hot transitions can easily be distinguished.[11] These Raman spectra revealed a richness of hot and (weak) combination and overtone bands of *trans*-formic acid, many of which have not been reported in the previous literature, particularly for the deuterated isotopologs. These data that are, in part, published[40,44] could not be fully analyzed and interpreted so far using available methods, such as standard VPT2. Particularly promising is the interpretation of hot bands as they are direct probes of anharmonicities. Naturally, the gas phase spectroscopy of *cis*-formic acid is more complicated due to the low abundance (one per mill) at room temperature.[25,45] The *cis* database[25] was significantly extended in recent years using the heatable Raman jet setup.[11,40,46] Our goal is to unify and summarize recent developments regarding the theoretical and experimental vibrational spectrum of *trans*-formic acid and its deuterated isotopologs below 4000 cm^{-1}.

This paper is structured as follows: We begin with discussing newly reported CVPT results, examining convergence, and comparing fundamental transition energies of both conformers to computational and experimental reference data. The main body of discussion is then centered around the assignment of new *trans*-formic acid peaks from Raman jet spectra and reassignment of literature IR bands. Finally, the two formic acid potential energy surfaces are compared.

II. METHODS

A. Experimental details

Using the same experimental protocol as before,[40] we have recorded new spectra to fill spectral gaps up to 3750 cm^{-1}. For experimental details, we therefore refer to Ref. 40. In short, different isotopologs of formic acid were seeded into helium and expanded at different temperatures through a vertical slit nozzle into an evacuated jet chamber. The expansion was probed with a continuous-wave 532 nm laser, which was operated at 20 W for the new measurements. The scattered light was collected perpendicular to the laser and nozzle flow and focused onto a monochromator, which disperses the photons onto a liquid nitrogen-cooled CCD-camera (1340 × 400 pixels) binning over 400 vertical pixels. To account for the final resolution from the combination of laser and monochromator, we generously assign band center errors of ±2 cm^{-1}. Spectra of a temperature series are intensity-scaled to a *trans*-formic acid fundamental in each spectral region. The advantage is that hot bands, i.e., transitions from thermally populated vibrational states, can be easily distinguished from the cold monomer and cluster bands as they increase in intensity with rising temperature, whereas the cluster bands decrease (for further reading, see Refs. 11 and 46). Overtone and combination bands of the *trans*-formic acid monomer can furthermore be distinguished as their intensity remains constant over a scaled temperature series, similar to fundamentals.

B. Potential energy surfaces

The two potential energy surfaces we use in this work are referred to as PES-2016[16] and PES-2018.[17] Both surfaces are full-dimensional and semi-global as they describe the *cis* and *trans* conformational space of formic acid. In the following, we briefly summarize technical aspects, and for details and references, see Refs. 16 and 17.

PES-2016 was presented by Tew and Mizukami in 2016. They fitted 17 076 single point energies at the CCSD(T)-F12c/VTZ-F12 level using a method similar to LASSO constrained optimization. Note that points along the O–H torsion as defined by the internal coordinate path were included in the fit. The potential is composed of a zero-order surface using Morse oscillators for the atom–atom distances to ensure proper asymptotic behavior. Perturbations are introduced by a more flexible correction surface that is a sum of distributed multivariate Gaussian functions of combinations of the atom–atom distances. The authors report an accuracy of the fit to 0.25% with a root-mean-square deviation of 9 cm^{-1} to the *ab initio* data in the energy range 0 cm^{-1}–15 000 cm^{-1}.

In 2018, Richter and Carbonnière presented a second full-dimensional formic acid potential, which they fitted to 660 single point energies at the CCSD(T)-F12a/aVTZ level using the AGAPES program. The potential is defined in a sum-of-product form using internal valence coordinates that minimize the potential energy coupling, e.g., the torsional motion is mostly localized along one dihedral coordinate. The AGAPES algorithm iteratively converges the potential energy expansion to a predefined cut-off value, in the process adding more *ab initio* points. The *dead branching* variant of AGAPES was used and the authors report the fit to be accurate between 0 cm^{-1} and 13 327 cm^{-1}.

C. Computational details on CVPT calculations

In this work, we solve the vibrational eigenstates and their corresponding eigenvalues using a numerical implementation of high order canonical Van Vleck perturbation theory (CVPT).[47–49] Our implementation requires a Hamiltonian expanded in terms of the normal coordinates and their conjugate momenta written in terms of raising and lowering operators.

The two potential surfaces we consider, as described above, are expanded in Taylor series in terms of the stretch, bend, and dihedral angles extensions following the coordinate choice of Richter and Carbonnière.[17] One difference is that we use Simons–Parr–Finlan coordinates for the stretches to improve the convergence properties.[50] The potential includes up to four-body terms. These contributions include expansion terms up to 8th, 6th, 6th, and 4th for the one- to four-body terms, respectively. A comparison of the torsional potentials and their fits is given in Fig. S13 of the supplementary material. The exact kinetic energy operator[51] is a function of the **G**-matrix elements. These elements are expanded through sixth order in the internal coordinates with the exception of four-body terms that are expanded through fourth order. The potential-like contribution to the kinetic energy[51] is expanded through fourth order.

The potential and kinetic contributions to the Hamiltonian are re-expressed in normal coordinates and conjugate momenta. The normal coordinates are curvilinear, since they are written as a linear expansion of the internal coordinates $\mathbf{R} = \mathbf{LQ}$, where $\mathbf{L}$ is obtained by diagonalization of the **F** and **G** matrices following the work of Wilson, Decius, and Cross.[52] As a final step, in order to carry out CVPT, the Hamiltonian is expressed in terms of the harmonic oscillator raising and lowering operators expressed in normal form.[53]

The CVPT is carried out through a series of transformations that order by order remove off-resonance terms. The details of the calculations have been described previously, so they are not repeated here.[53,54] The central point is that the more off-diagonal terms that are removed, the poorer the agreement between subsequent orders of perturbation theory and the smaller the sizes of the matrices that need to be diagonalized. The two extremes are a final effective Hamiltonian that equals the initial Hamiltonian and a Hamiltonian with no coupling terms. There are many criteria that are used in deciding the form of the final Hamiltonian.[47,55,56] In this work, we follow an approach that was successful for describing the vibrations of HFCO,[54] a molecule with many possible resonances. In that approach, a rather large list of possible resonance terms is generated. Our criteria are based solely on energy mismatch; coupling strength is not considered. If a coupling term couples states with an energy difference less than W_i/cm^{-1}, where i is the order of the coupling terms, then the coupling term is retained. Here, we set $\{W_3, W_4, \ldots, W_8\} = \{350, 200, 60, 50, 15, 15\}$ and therefore retain many small coupling terms that could be transformed away, knowing that these terms are readily treated in the ensuing variational calculation of the transformed Hamiltonian.

The resulting transformed Hamiltonian is expressed as a matrix using a product basis of harmonic oscillators. The size of this basis is constrained by the number of quanta in each oscillator. We use the constraint $\sum_i c_i n_i \le N_t$, where $\mathbf{c} = \{1, 2, 2, 2, 3, 3, 6, 6\}$ when the modes are ordered in terms of increasing frequency and $N_t = 8$. These numbers are roughly based on the frequencies and have not been optimized in a systematic way. These values lead to modest-sized matrices of 264 and 213 for *trans*-formic acid for the two symmetry blocks, respectively. Comparing results to $N_t = 12$ shows that all states are converged to better than 0.1 cm^{-1} compared to the smaller bases for the sixth order CVPT results of *trans*-formic acid. Our approach allows for many possible resonance interactions through the large values of **W** that still yield representations for which the eigenfunctions of the effective Hamiltonians can be readily obtained.

In order to test the quality of the results, it is important to compare eigenvalues calculated at different orders of perturbation theory. We do this by comparing $E(4)$ results to $E(6)$ results where the order of the perturbative result is in parentheses. If one finds significant discrepancies, we consider the possible terms that are leading to the slow convergence and adjust the values of **W** accordingly. Atomic masses used in the CVPT calculations are reported in the supplementary material.

III. CVPT RESULTS

A. Convergence of CVPT eigenstates

The convergence of newly reported CVPT vibrational eigenvalues is quantified with the three quantities $\{E_{\max}, n_{\max}, N_{\text{ord}}\}$, where N_{ord} is the order of perturbation theory and the other two parameters identify the states included in the comparison set. We set $E_{\max} = 4000$ cm^{-1} and $n_{\max} = 4$, constraining states to have energies below the cut-off energy $E_{\max}$ and $\sum_i n_i \le n_{\max}$. The state identification is based on the leading coefficient in the expansion.

Convergence with respect to the level of perturbation theory is shown in Fig. 2 for *trans*- and *cis*-HCOOH where the energy difference between sixth and second as well as sixth and fourth order

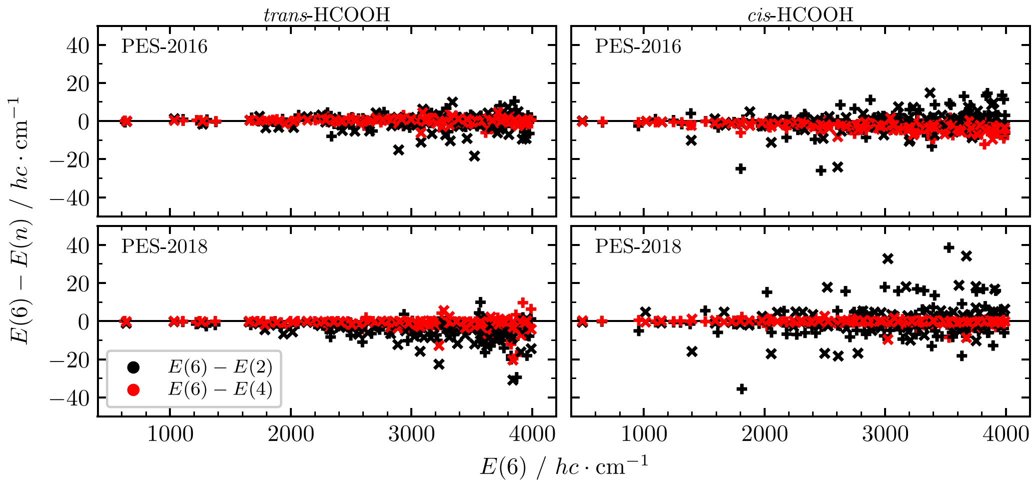

FIG. 2. Convergence plots for *trans*- (left) and *cis*-HCOOH (right) vibrational states relative to their respective ground state energy using canonical Van Vleck perturbation theory (CVPT). States of a' and a'' symmetry are marked as "+" and "×," respectively. Convergence is quantified with the quantities $\{E_{\mathrm{max}}, n_{\mathrm{max}}, N_{\mathrm{ord}}\}$, where N_{ord} is the order of perturbation theory, E_{max} is the maximum allowed $E(6)$ energy in cm^{-1}, and n_{max} is the maximum sum of quanta of vibrational excitation for states included in the comparison set. Energy differences between sixth and second as well as sixth and fourth order states are shown for E_{max} = 4000 and n_{max} = 4.

states is compared. In comparing two orders of perturbation theory, we compare states that are most similar to each other, and we use their overlap as a measure of this similarity. As an example, the overlap between the fourth order and sixth order states is defined by $\mathbf{S} = \mathbf{U}_4^T \mathbf{U}_6$, where $\mathbf{U}_n^T \mathbf{H}_n \mathbf{U}_n$ is the similarity transformation that diagonalizes the nth order Hamiltonian. At low energies, the diagonal elements S_{ii} are close to one. Whenever eigenvalues switch order between two levels of perturbation theory or if two states are in resonance at one level and not at another, then this information is encoded in the elements of $\mathbf{S}$ and can be used to match the states appropriately.

Figure 2 (left panels) shows that vibrational eigenstates of *trans*-HCOOH on PES-2016 are slightly better converged than on PES-2018. On the whole, the deviation between fourth and sixth order shows that eigenstates are converged within a few cm^{-1}. The convergence of individual states can be checked with data provided in Table S7 of the supplementary material. The mean absolute deviation (maximum absolute deviation) for n_{max} = 1, 2, 3, 4 states is below 1(2), 1(3), 1(6), and 2(7) on PES-2016 and below 1(5), 1(5), 2(13), and 3(21) on PES-2018, all in units of cm^{-1}. The comparison between sixth and second order is especially insightful as second order Van Vleck perturbation theory is the same as standard VPT2[57] with resonance treatment (VPT2+K).[58] On PES-2016, the performance for fundamentals and binary states is quite satisfactory with mean absolute deviations (maximum absolute deviations) below 1(3) cm^{-1} and 2(6) cm^{-1}, respectively. The limitations of VPT2+K are revealed beyond two quanta where the maximum absolute deviations to sixth order CVPT amount to 19 cm^{-1} and 16 cm^{-1} for three- and four-quantum states, respectively (cf. Table S7).

The CVPT calculated fundamentals, as well as states with multiple quanta of excitation, converge more slowly for *cis*-formic acid on PES-2016 than PES-2018, which is reflected in Fig. 2 (right panels). Fundamental wavenumbers of *cis*-HCOOH are converged within 1 cm^{-1} with respect to the order of perturbation on PES-2018, whereas the two high-frequency X–H stretching fundamentals on PES-2016 differ by 4 cm^{-1} between fourth and sixth order. As expected, the O–H torsion of formic acid is very sensitive to the relative conformation, as reflected in the large down-shift from 640.73 cm^{-1} to 493.42 cm^{-1} for the fundamental. The frequency lowering reduces the involvement of the torsion in strong resonance polyads—groups of nearly degenerate states that are described as zero-order coupled states[59]—which are characteristic of the *trans* species (*vide infra*).[14] This decoupling for *cis* appears to improve the convergence of the remaining higher-frequency low-lying states so that overall CVPT converges faster for *cis* than *trans*, as can be observed by comparing the left- and right-hand side panels of Fig. 2.

B. Comparison of computed and experimental fundamental transition energies

The nine vibrations of *trans*-formic acid are schematically shown in Fig. 3. These localized representations are idealized, especially the C–H/D and O–H/D in-plane bending, and C–O stretching vibrations ν_4, ν_5, and ν_6 are mixed group vibrations. In this work, we apply the Herzberg nomenclature of HCOOH also to its three deuterated isotopologs. With a large number of perturbation-free experimental reference data available for fundamentals of both conformers, we can compare PES-2016 and PES-2018 using different anharmonic vibrational methods such as the internal coordinate path Hamiltonian (ICPH),[16] multi-configuration time-dependent Hartree (MCTDH),[17,18] and high order canonical Van Vleck perturbation theory (CVPT).

The anharmonic fundamentals of HCOOH are listed together with experimental reference data in Table I; deviations between

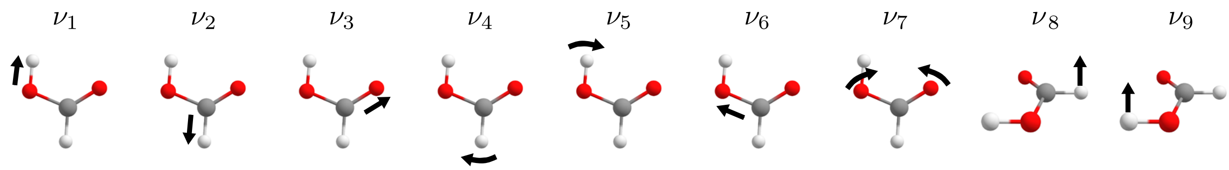

FIG. 3. Schematic drawings of fundamental vibrations of *trans*-HCOOH. In this work, we apply the Herzberg nomenclature of *cis*- and *trans*-HCOOH to all their three deuterated isotopologs.

experiment and anharmonic calculations employing both PES are visualized in Fig. 4. These figure results include all deuterated isotopologs. Table I shows that the CVPT6 results for *trans*-HCOOH compare favorably with ICPH and MCTDH reference data on the same surface as they agree within 2 cm^{-1}. Comparison for *cis*-HCOOH indicates that the internal coordinate path Hamiltonian (ICPH) eigenvalues are not fully converged. In addition, the CVPT6/PES-2016 calculation overestimates the O–H stretch $\nu_1(cis)$ transition energy by 16 cm^{-1}. Given that CVPT4 and CVPT6 agree within 4 cm^{-1}, this discrepancy is probably due to the surface. Note that $\nu_1(cis)$ was not reported in Ref. 16 and is therefore missing in Fig. 4. MCTDH and CVPT6 results for *cis* compare favorably with deviations below 3 cm^{-1} except for ν_1, which differs more (3631 cm^{-1} MCTDH, 3636 cm^{-1} CVPT6). Upon C–H deuteration,[18] ν_1 agreement between MCTDH (3625 cm^{-1}) and CVPT6 (3637 cm^{-1}) worsens where the MCTDH predictions seem somewhat more sensitive to isotopic substitution (−6 cm^{-1}, +1 cm^{-1} CVPT6) than the experimental data indicate (−2 cm^{-1}). On the whole, Fig. 4 demonstrates that vibrational energies for both conformers tend to be higher than experiment on PES-2016, whereas PES-2018 tends to underestimate the experiment.

The careful reader will have noticed that in Fig. 4, data for 35 instead of 4 × 9 = 36 *trans* fundamentals are shown. To this day, the C–H out-of-plane vibration ν_8 of HCOOD remains the only fundamental not reported in the gas phase. The anharmonic calculations on PES-2016 and PES-2018 consistently predict ν_8 to be slightly shifted down by 1 cm^{-1}–2 cm^{-1}

TABLE I. Fundamentals of *cis*- and *trans*-HCOOH computed using PES-2016 and PES-2018 together with experimental values (see Ref. 40 and references therein).

Fundamental		PES-2016		PES-2018		
Label	Γ	ICPH[16]	CVPT6	MCTDH[17]	CVPT6	Exp.
cis-HCOOH						
ν_1	a'	n.r.	3653	3631	3636	3637
ν_2	a'	2880	2878	2871	2874	2873
ν_3	a'	1824	1821	1810	1810	1818
ν_4	a'	1394	1389	1383	1384	
ν_5	a'	1255	1246	1246	1247	
ν_6	a'	1103	1096	1097	1097	1093
ν_7	a'	668	657	652	652	
ν_8	a''	1038	1020	1011	1014	
ν_9	a''	492	491	491	491	493.42
trans-HCOOH						
ν_1	a'	3575	3576	3567	3568	3570.5
ν_2	a'	2938	2940	2937	2939	2942.06
ν_3	a'	1783	1783	1774	1773	1776.83
ν_4	a'	1379	1380	1375	1374	1379.05
ν_5	a'	1305	1305	1301	1300	1306.2
ν_6	a'	1108	1108	1106	1106	1104.85
ν_7	a'	627	627	623	623	626.17
ν_8	a''	1034	1035	1032	1032	1033.47
ν_9	a''	638	640	637	637	640.73

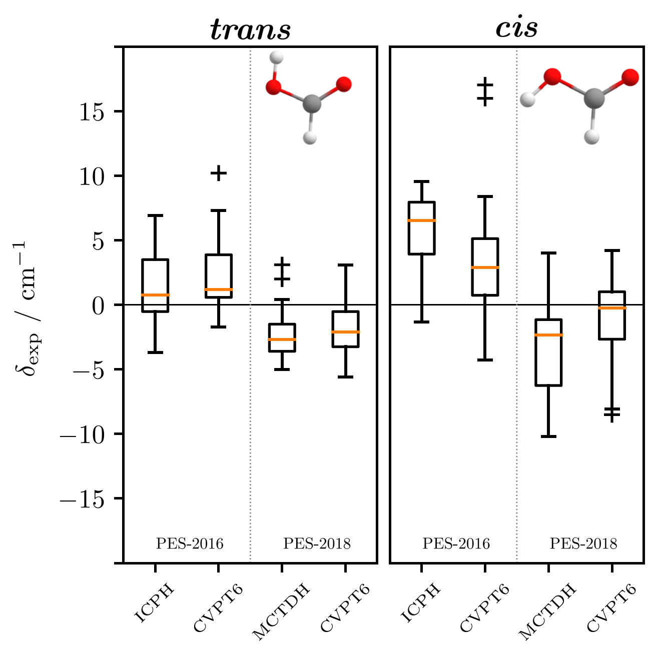

FIG. 4. Deviation between experimental and computed formic acid fundamental wavenumbers ($\delta_{exp} = \tilde{\nu}_{calc} - \tilde{\nu}_{exp}$). Data for all four H/D isotopologs are aggregated for *cis*- and *trans*-formic acid with 16 and 42 data points, respectively. These 42 points comprise 35 *trans* fundamentals and their resonance partners including $2\nu_9$ (HCOOH), $2\nu_8$ and $2\nu_9$ (DCOOH), $\nu_3 + \nu_6$ and $2\nu_9$ (HCOOD), and $\nu_4 + \nu_6$ and $2\nu_8$ (DCOOD). For the ICPH model, 8 and 10 data points are used, respectively, as ν_1 of *cis* is not reported in Ref. 16 and deuterated data are not available. Each box extends from the lower quartile to the upper quartile of the data, and whiskers extend out to twice the interquartile range. Outliers are marked as crosses (+), and each box is bisected by a line indicating the median.

upon O-D isotopic substitution. Experimental data in a weakly perturbing neon matrix indicate a similar shift in the opposite direction, however.[3,10] Both overtones could be observed in this work at 2060 cm^{-1} (HCOOH) and 2055 cm^{-1} (HCOOD). The overall weak experimental band integrals and "pure" CI coefficients (>0.99) indicate $2\nu_8$ not to be perturbed (significantly) by resonances, as is the case for DCOOH and DCOOD (cf. Table IV and Fig. S9). In the context of second order perturbation theory,[57]

$$\frac{E(\mathbf{n})}{hc} = \sum_i \tilde{\omega}_i\left(n_i + \frac{1}{2}\right) + \sum_{i\geq j} x_{i,j}\left(n_i + \frac{1}{2}\right)\left(n_j + \frac{1}{2}\right), \tag{1}$$

one can extract an $x_{i,i}$ value if one knows the transition energy of both the fundamental and first overtone of the ith mode. Using the fundamental (1033.47 cm^{-1} from Ref. 7) and first overtone (2060 cm^{-1}) of *trans*-HCOOH, one obtains a diagonal anharmonicity constant of $2x_{8,8} = -7$ cm^{-1}. Assuming $x_{8,8}$ to remain unchanged upon O-D isotopic substitution, the gas phase band center of *trans*-HCOOD can be estimated to be shifted down by 2 cm^{-1} relative to *trans*-HCOOH, in line with anharmonic predictions (Table IV).

IV. (RE)ASSIGNMENT OF *TRANS*-FORMIC ACID BANDS

While *trans*-HCOOH experimental vibrational data are available up to 14 000 cm^{-1} (Ref. 7) and select OH overtone data beyond,[64] we restrict our discussion in this work to vibrational levels up to 4000 cm^{-1}. On the basis of the available calculations and symmetry information from depolarized Raman spectra, we assign peaks in the Raman jet spectra reported in Refs. 40 and 44 and this work and review previously assigned IR bands. As some of the reassignments make use of depolarization ratios, we give a brief explanation of depolarization ratios and their relation to the symmetry of a vibration as note in the references.[65] For further reading, see Refs. 66 and 67.

In order to motivate these assignments, we have examined a wide range of data. We have compiled available benchmark quality, i.e., perturbation-free, experimental reference data from the literature and show them together with Raman jet band centers in Table II for HCOOH; data for the deuterated isotopologs are shown in Appendix B (Table IV). Newly assigned bands are marked with an asterisk and assignments that deviate from Refs. 16 and 17 (or

TABLE II. Vibrational wavenumbers (in cm^{-1}) of *trans*-HCOOH states with one or two vibrational quanta. Other states are included if they are involved in resonances or assignments of experimental bands. Internal coordinate path Hamiltonian (ICPH),[16] multi-configuration time-dependent Hartree (MCTDH),[17] and canonical Van Vleck perturbation theory (CVPT) predictions using two different analytical PES[16,17] are shown together with perturbation-free experimental data. The asterisk denotes newly assigned bands, and the dagger denotes a reassignment. Tentative assignments are in brackets, not fully converged MCTDH energies are set in parentheses (adopted from Ref. 17), and energy levels obtained from hot band assignments are italicized. Numbers in the state labels refer to the vibrational degree of freedom, which is indexed with the respective quanta of excitation.

	State		Exp.		PES-2016[a]		PES-2018[b]	
	Label	Γ	Ra. jet[c]	Lit.	ICPH	CVPT6	MCTDH	CVPT6
	7_1	a'	626	626.17[d]	627	627	623	623
	9_1	a''		640.73[d]	638	640	637	637
	8_1	a''		1033.47[e]	1034	1035	1032	1032
	6_1	a'	1104	1104.85[e]	1108	1108	1106	1106
	9_2	a'	1220	1220.83[f]	1222	1221	1216	1216
	7_2	a'		1253.44[g]	1256	1256	1247	1246
	7_19_1	a''		1268.69[g]	1268	1269	1261	1260
	5_1	a'	1306	1306.2[h]	1305	1305	1301	1300
	4_1	a'	1379	1379.05[i]	1379	1380	1375	1374
	7_18_1	a''			1661	1661	1654	1655
*	8_19_1	a'	1673		1672	1675	1668	1668
†	6_17_1	a'	*1727*	1726.40[j]	1733	1732	1725	1725
†	6_19_1	a''	*1738*	1737.96[j]	1739	1741	1736	1736
	3_1	a'	1776	1776.83[j]	1783	1783	1774	1773
	9_3	a''		1792.63[j]	1795	1793	1786	1786
	7_19_2	a'	1847	1847.8,[h] 1843.48	1855	1850	1839	1839
	5_17_1	a'	1931	1931.1[h]	1933	1932	1922	1921
*	5_19_1	a''	*1951*		1947	1950	1943	1942
	4_17_1	a'			2006	2006	1998	1997
	4_19_1	a''			2021	2024	2016	2014
*	8_2	a'	2060		2063	2066	2058	2060
	6_18_1	a''		2132[h]	2139	2139	2134	2135

TABLE II. (*Continued.*)

	State		Exp.		PES-2016[a]		PES-2018[b]	
	Label	Γ	Ra. jet[c]	Lit.	ICPH	CVPT6	MCTDH	CVPT6
	6_2	a'	2197	2196.3[h]	2205	2204	2200	2199
†	9_4	a'	[2298]	[2298.6][h]	2312	2305	2294	2295
*	$7_1 8_1 9_1$	a'	[2301]		2302	2304	2291	2292
†	$6_1 9_2$	a'	2336	[2338][h]	2358	2338	2332	2331
	$5_1 8_1$	a''			2338	2338	2330	2331
	$6_1 7_1 9_1$	a''		[2376][h,k]	2369	2368	2357	2356
*	$3_1 7_1$	a'	2395		2402	2402	2390	2389
†	$5_1 6_1$	a'	2400	2400.2[h]	2406	2405	2398	2396
	$3_1 9_1/7_1 9_3$	a''			2420	2418	2404	2405
*	$3_1 9_1/7_1 9_3$	a''	*2424*		2447	2427	2414	2413
	$4_1 8_1$	a''			2415	2416	2408	2407
	$4_1 6_1$	a'			2479	2479	2473	2473
	$5_2/5_1 9_2$	a'	2504	2504[h]	2511	2507	2498	2499
	$5_2/5_1 9_2$	a'			2608	2608	2598	2595
	$4_1 9_2$	a'		[2600][h]	2600	2598	2589	2588
*	$4_1 5_1$	a'	2678		2678	2678	2670	2669
	4_2	a'	2746	2745[h]	2746	2747	2738	2736
	$3_1 8_1$	a''		2803[h]	2810	2810	2801	2800
	$3_1 6_1$	a'		2876.6[h]	2886	2884	2875	2874
	2_1	a'	2942	2942.06[h]	2938	2940	2937	2939
*	$7_1 9_4$	a'	2960		3066	2964	2950	2952
	$5_1 7_1 8_1$	a''			2965	2965	2951	2952
*	$3_1 9_2$	a'	2995		3003	3002	2989	2987
	$4_1 8_1 9_1$	a'		[3057][h]	3058	3061	3047	3046
	$3_1 5_1$	a'	3081	3083[l]	3087	3087	3075	3073
	$4_1 6_1 7_1$	a'		[3106.5][h]	3105	3103	3093	3092
	$4_1 6_1 9_1$	a''			3115	3117	3108	3105
	$3_1 4_1$	a'	3153	3152.3[h]	3161	3160	(3086)	3145
	6_3	a'		[3275][h]	3292	3289	n.r.	3281
	3_2	a'	*3533*	3538/3533[m]	3547	3545	3530	3529
	[1_1-Res]	a'	3559					
*	$2_1 7_1$	a'	3567		3566	3568	3558	3561
	1_1	a'	3570	3570.5[h]	3575	3576	3567	3568
	$2_1 9_1$	a''			3579	3581	n.r.	3575
	[1_1-Res]	a'	3609					
†	$3_1 8_2$	a'		3826[h]	3833	3835	n.r.	3821
	$4_2 6_1$	a'			3836	3835	n.r.	3825
*	$2_1 8_1$	a''	*3958*		3952	3954	n.r.	3954
†	$3_1 6_2$	a'		[3963.6][h]	3978	3975	n.r.	3963

[a]Reference 16, taken from the respective supplementary material.
[b]Reference 17.
[c]Fundamentals and resonance partners from Ref. 40 and Raman peak at 2960 cm^{-1} from Ref. 44; otherwise, this work.
[d]Reference 20.
[e]Reference 60.
[f]Reference 61.
[g]Computed from parameters reported in Ref. 8.
[h]Reference 7.
[i]Reference 62.
[j]Reference 9.
[k]Probably not corresponding to a ground state *trans*-HCOOH transition; see the text for discussion.
[l]Reference 42.
[m]Reference 63.

the experimental reference if not discussed in either) are indicated by a dagger. (Re)Assignments are based on the combined predictions from ICPH,[16] MCTDH,[17,18] and CVPT6 calculations and taking into account the expected error progression for each state. We use the deviation between the experiment and calculation for a fundamental as a measure of the error associated with this vibrational degree of freedom per quantum of excitation. In the following, we discuss (re)assignments concerning *trans*-HCOOH and touch upon deuterated isotopologs whenever necessary for the interpretation of HCOOH bands. Convergence data and CI mixing coefficients are shown for states relevant to the discussion in Appendix A (Table III). The Raman jet spectra in the full spectral range between 870 cm^{-1} and 3750 cm^{-1} are shown in Figs. S1–S12 of the supplementary material. The discussion of (re)assignments is sorted by energy, starting with the low-frequency end of the spectrum. The O–H stretching spectrum between 3510 cm^{-1} and 3630 cm^{-1} is discussed separately at the end.

A. Formic acid spectrum below 2150 cm^{-1}

The first reassignment in Table II, as indicated by the daggers (†), concerns the bands at 1727 cm^{-1} and 1738 cm^{-1}. These bands are assigned as the combination bands $\nu_6 + \nu_7$ and $\nu_6 + \nu_9$, respectively. One might expect the latter to be higher in energy since ν_7 lies below ν_9. However, Perrin *et al.* analyzed several interacting states in the ν_3 region by high-resolution IR spectroscopy and fitted ro-vibrational lines with an effective Hamiltonian. They reported (among others) band centers at 1726.40 cm^{-1} and 1737.96 cm^{-1} for $\nu_6 + \nu_9$ and $\nu_6 + \nu_7$, respectively.[9] This "inverse" order was attributed to resonance interactions with ν_3 shifting $\nu_6 + \nu_7$ above $\nu_6 + \nu_9$; the latter can only interact via Coriolis couplings, while the former can additionally interact via Fermi couplings. In contrast, all four calculations in Table II indicate that the naive assignment based on the order of fundamentals is correct as was recognized by Richter and Carbonnière. They had proposed a reassignment based on improved root-mean-square deviations among both ICPH and MCTDH calculations.[17] Moreover, we find that the above postulated Fermi coupling is small, being on the order of 1 cm^{-1}, this providing further evidence that the lower band should be assigned to $\nu_6 + \nu_7$.

Coincidentally, in the Raman jet spectrum of HCOOH, peaks at 1737 cm^{-1} and (much weaker) at 1726 cm^{-1} are observed, and *both* correspond to a' transitions. The agreement with the band assigned to $\nu_6 + \nu_7$ by Perrin *et al.*, however, is coincidental, as the Raman signal at 1737 cm^{-1} can be ascribed to ν_3 of $H^{13}COOH$ due to the naturally occurring ^{13}C isotope. The isotope shift was measured in the gas phase[23] and weakly perturbing neon matrix,[3] amounting to −40 cm^{-1}, in perfect agreement with the observed −39 cm^{-1}. The corresponding ^{13}C peak can also be identified in the HCOOD spectrum at 1733 cm^{-1}, shifted by −39 cm^{-1}. Using CVPT6 predictions, we can furthermore identify one band of the $\nu_3/2\nu_8$ doublet for C-deuterated and even ν_6 for O-deuterated isotopologs of formic acid-^{13}C. Band centers are tabulated in Table S3 of the supplementary material

For further confirmation that the ro-vibrational lines observed by Perrin *et al.*, that correspond to a band center at 1726 cm^{-1}, should be assigned to $\nu_6 + \nu_7$, we turn to hot bands involving the two energy levels in question. Although we cannot observe $\nu_6 + \nu_9$ directly in the Raman spectrum of HCOOH, we can calculate hot bands of ν_6 originating from the two (by far) lowest energy levels ν_7 and ν_9 using experimental data and compare those results with the observed hot bands in Fig. 5. With the assignment by Perrin *et al.*, we expect one hot band to be blue-shifted (+6.94 cm^{-1}) and one red-shifted (−19.18 cm^{-1}) relative to the ν_6 fundamental. In the Raman spectrum, three distinctly separated hot bands can be found, shifted from the fundamental by −3 cm^{-1}, −7 cm^{-1}, and −11 cm^{-1}—all three red-shifted from ν_6—where the latter was assigned to ν_6 of *cis*-HCOOH by Meyer and Suhm.[11,40] An assignment of $\nu_6 + \nu_7$ and $\nu_6 + \nu_9$ inverse to Perrin *et al.*, however, would yield shifts of −4.62 cm^{-1} and −7.62 cm^{-1}, which are compatible with the observed hot band structure as was recognized by Meyer[44] and which is consistent with all anharmonic predictions. We therefore confirm the reassignment proposed by Richter and Carbonnière.

Contrary to HCOOH, the hot band structure around the C–O stretching fundamental ν_6 is much more complicated for DCOOH, featuring much less intensity but an overall higher density of peaks and a blue-shifted hot band. In the absence of anharmonic Raman intensities, we simulate the ν_6 spectrum using a simple model assigning a linear transition term to the C–O stretch. The experimental and simulated spectra using CVPT6/PES-2016 anharmonic energies are compared for all four H/D isotopologs in Fig. 5. We scale the *trans* fundamental with 3/20 to reproduce the relative experimental intensities and shift the wavenumber axis to match experiment. For the *cis* fundamental, the scaled transition oscillator strength of the *trans* fundamental is multiplied with the appropriate Boltzmann factor and the relative *cis*–*trans* Raman intensity factor from Ref. 40 (ESI, Table S3).

Considering the crudeness of the model, the simulated spectra predict the relative intensities and band contours between

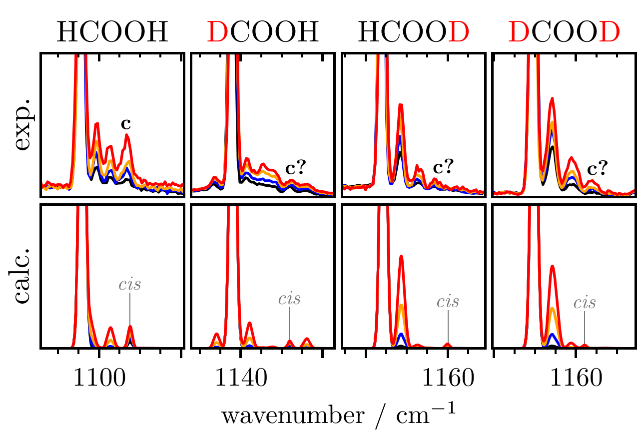

FIG. 5. Calculated hot band progressions in the vicinity of the C–O stretch ν_6 are compared to the Raman jet spectra of formic acid (acid-in-helium concentration <0.2%–0.4%). Wavenumber ticks are separated by 5 cm^{-1}. To compare the relative hot band intensities, the limits on the y-axis are set to 1/3 of the maximum intensity of ν_6 for each isotopolog. The width of the Gaussian functions is set to $\sigma = \sqrt{0.5}$ to roughly match the experiment. See the text for details on computed intensities.

different isotopologs surprisingly well. Note that the choice of width for the Gaussian functions and the underestimated redshift for $\nu_6 + \nu_7 - \nu_7$ (simulation −2 cm^{-1}, experiment −4 cm^{-1}) causes the hot band for HCOOH to overlap with the fundamental peak in Fig. 5. Hot bands originating from ν_7 and ν_9 overlap for O-deuterated formic acid and an accidental resonance between $\nu_6 + \nu_9$ and $3\nu_9$ causes $\nu_6 + \nu_9 - \nu_9$ to be shifted above the fundamental for DCOOH. With a refined model including higher (anharmonic) terms in the polarizability tensor, it seems possible to assign $\nu_6(cis)$ for all three deuterated isotopologs in the Raman jet spectra shown in Fig. 5.

From the above mentioned ro-vibrational analysis of ν_3, Perrin *et al.* obtained band centers for several interacting states by simultaneously fitting the interacting vibrational states ν_3, $\nu_6 + \nu_7$, $\nu_6 + \nu_9$, $3\nu_9$, and $\nu_7 + 2\nu_9$ (the latter two originally labeled $\nu_5 + \nu_9$ and $\nu_5 + \nu_7$, respectively).[9] We find that our Raman band centers for the $\nu_5 + \nu_7/\nu_7 + 2\nu_9$ Fermi doublet at 1931 cm^{-1} and 1847 cm^{-1} agree well with band centers reported by Freytes *et al.* at 1931.1 cm^{-1} and 1847.8 cm^{-1} (originally assigned to $3\nu_7$ and $\nu_5 + \nu_7$, respectively), which were also determined from the respective *Q* branches.[7] The band center that Perrin *et al.* reported at 1843.48 cm^{-1},[9] however, significantly deviates from the high-resolution IR value reported by Freytes *et al.* This discrepancy may be resolved by updating the state assignments and therefore the form of the off-diagonal coupling elements in the fit Hamiltonian.

So far, the discussion has focused on the assignment of peaks that *are* observed in the Raman jet spectrum. Looking at Table II, it is surprising that while the two-quantum states $\nu_5 + \nu_7$ (1931 cm^{-1}) and $2\nu_8$ (2060 cm^{-1}) are observed, the state $\nu_4 + \nu_7$, which is predicted to lie between the two, is not. Following the method by Dübal and Quack,[59,68] we analyze nearby a' symmetric states for the CI contribution of the ν_3 fundamental to the respective state, assuming that "dark" states gain intensity via resonance mixing with ν_3. The CVPT6/PES-2016 calculation predicts contributions of ν_3 to seven other states with squared CI coefficients of 0.87% ($\nu_7 + 2\nu_9$), 0.31% ($2\nu_8$), 0.30% ($\nu_5 + \nu_7$), 0.16% ($\nu_8 + \nu_9$), 0.09% ($\nu_6 + \nu_7$), 0.02% ($3\nu_7$), and 0.01% ($\nu_4 + \nu_7$). This simple model satisfactorily explains the absence of $\nu_4 + \nu_7$, $3\nu_7$, and the very weak intensity of $\nu_6 + \nu_7$. In analogy, it further illustrates the absence of $2\nu_7$, which has a total contribution below 0.1% from the much weaker (relative to ν_3) fundamentals ν_4, ν_5, and ν_6, and the general lack of a'' symmetric combination/overtones (cf. Tables II and IV). The (un)observed peak structure of the Raman jet spectrum of *trans*-HCOOH up to 2150 cm^{-1} can entirely be understood within this simple model where "bright" fundamentals light up nearby dark states via (weak) resonance mixing.

B. Formic acid spectrum between 2150 cm^{-1} and 2500 cm^{-1}

Segments of the HCOOH and DCOOH Raman jet spectra between 2210 cm^{-1} and 2450 cm^{-1} are shown together with CVPT6 predictions on both surfaces in Fig. 6 to aid the following discussion. In this spectral window, four HCOOH bands are reported by Freytes *et al.* at 2400.2 cm^{-1}, 2376 cm^{-1}, 2338 cm^{-1}, and 2298.6 cm^{-1}. We propose reassignments in all four cases.

The initial assignment of the band at 2400.2 cm^{-1} to $2\nu_5$ by Freytes *et al.* was rejected by Tew and Mizukami as well as Richter and Carbonnière on the grounds that their calculations predict $2\nu_5$ at much higher energies.[16,17] Richter and Carbonnière

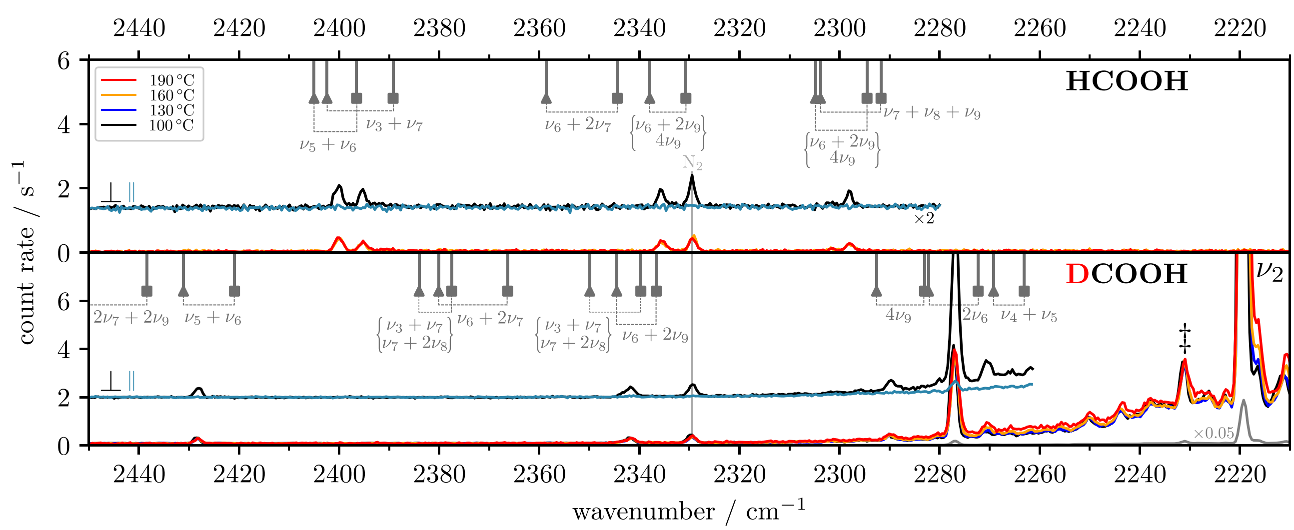

FIG. 6. Raman jet spectra of HCOOH and DCOOH in helium (<0.3% and <0.4%, respectively) between 2210 cm^{-1} and 2450 cm^{-1}. For each isotopolog, the spectra of a temperature series have been intensity-scaled to a *trans* fundamental (for HCOOH not shown) with the lowest intensity among all temperatures. Isotopic impurities are marked with a double dagger (‡). For DCOOH, the 160 °C spectrum is additionally shown further intensity-scaled (×0.05) in gray. Additional depolarized spectra at 190 °C are shown with the incident laser polarization perpendicular (⊥, black, default for all other measurements) and parallel (∥, cyan) with respect to the scattering plane. CVPT6 predictions using PES-2016 (▲) and PES-2018 (■) are shown as gray sticks for states of a' symmetry between 2230 cm^{-1} and 2450 cm^{-1}.

pointed out that taking into account the expected error progression of the two possible candidates $\nu_3 + \nu_7$ and $\nu_5 + \nu_6$, the latter is a better match since the former is expected at slightly lower energies around 2395 cm^{-1}–2396 cm^{-1}. We can confirm this reassignment as we observe two bands in our Raman spectra at 2400 cm^{-1} and 2395 cm^{-1}, which we assign to $\nu_5 + \nu_6$ and $\nu_3 + \nu_7$, respectively.

By re-visiting early IR studies on formic acid with high quality anharmonic calculations, we are also able to assign $\nu_5 + \nu_6$ for *trans*-HCOOD. In one of the first spectroscopic investigations of deuterated formic acid monomer, Williams reported two bands of *trans*-HCOOD at 2178.8 cm^{-1} and 2142.4 cm^{-1}, which he could not assign.[69] Nearly 70 years later, these bands remain unassigned, as far as we know. Using the anharmonic predictions on both PESs (Tables III and IV), the lower energy band can either be assigned to $\nu_5 + \nu_6$ or $2\nu_7 + \nu_8$ and the higher energy band to $\nu_6 + 2\nu_9$ or $3\nu_7 + \nu_9$, where $\nu_5 + \nu_6$ and $\nu_6 + 2\nu_9$ are predicted to be strongly coupled on the basis of their respective CI coefficients. The best energy matches for the bands at 2142.4 cm^{-1} and 2178.8 cm^{-1}, and further confirmed by correction for expected error progression, are $\nu_5 + \nu_6$ and $\nu_6 + 2\nu_9$, respectively. $\nu_5 + \nu_6$ of *trans*-HCOOD was reported by Marushkevich *et al.* at 2139.8 cm^{-1} and 2176.8 cm^{-1} in neon and 2144.1 cm^{-1} and 2181.0 cm^{-1} in argon matrices—the similarity to the gas phase band centers introduces the possibility of interpreting the matrix data as the Fermi pair $\nu_5 + \nu_6$ and $\nu_6 + 2\nu_9$, as opposed to a matrix site effect.[70]

The band at 2376 cm^{-1} was initially assigned by Freytes *et al.*[7] to $\nu_3 + \nu_7$ and tentatively reassigned by Tew and Mizukami to $\nu_6 + \nu_7 + \nu_9$.[16] Since $\nu_3 + \nu_7$ is assigned to 2395 cm^{-1}, this leaves $\nu_6 + \nu_7 + \nu_9$ as the only plausible assignment considering that the energetically next higher state is predicted to be greater than 2410 cm^{-1}. Even taking into account expected error progressions, the predictions are still 9 cm^{-1}–14 cm^{-1} below experiment. Based on the remarkable agreement with experiment for states up to three and four quanta, and as we shall see below, even for states involving resonances, this assignment seems unlikely, and we believe that this band does not correspond to a ground state *trans*-HCOOH transition.

A critical reassignment concerns the two IR bands at 2338 cm^{-1} and 2298.6 cm^{-1}.[7] Freytes *et al.* assigned the latter tentatively to $\nu_5 + \nu_6$, which we have already reassigned to 2400.2 cm^{-1}. Tew and Mizukami reassigned both bands to $\nu_5 + \nu_8$ (a'') and $\nu_7 + \nu_8 + \nu_9$ (a'),[16] respectively; Richter and Carbonnière noted that in light of their MCTDH results, alternative reassignments to $4\nu_9$ (a') and $\nu_6 + 2\nu_9$ (a') seem plausible.[17] In the Raman spectrum of *trans*-HCOOH (Fig. 6, top), we observe three peaks at 2336 cm^{-1}, 2301 cm^{-1}, and 2298 cm^{-1}, all of which correspond to totally symmetric a' transitions. This yields three or four bands in this spectral region, depending on whether the band Freytes *et al.* observed at 2338 cm^{-1} corresponds with the signal we observe at 2336 cm^{-1}—the deviation of 2 cm^{-1} is just within our experimental resolution of ±2 cm^{-1}. The ICPH calculation cannot explain the a' band at 2336 cm^{-1}, since the "best match" $\nu_5 + \nu_8$ can be ruled out by symmetry considerations. The energetically next possible candidates are $4\nu_9$ at 2358 cm^{-1} and $\nu_6 + 2\nu_9$ at 2312 cm^{-1}, which (even after expected error correction) are energetically too far away to plausibly be assigned to the Raman peak at 2336 cm^{-1}. Looking at Table II, it can be seen that the MCTDH predictions using PES-2018 are compatible with the CVPT results on PES-2016; CVPT and MCTDH predict the two aforementioned states $4\nu_9$ and $\nu_6 + 2\nu_9$ to be strongly coupled where the higher energy band is predicted between 2331 cm^{-1} and 2338 cm^{-1} and the lower energy band between 2294 cm^{-1} and 2305 cm^{-1}.

We can gain further insights by turning to the Raman spectrum of DCOOH, as the CVPT calculations indicate that this resonance persists upon C–H deuteration. In the same spectral region, we observe five a' bands at 2428 cm^{-1}, 2342 cm^{-1}, 2290 cm^{-1}, 2277 cm^{-1}, and 2271 cm^{-1}. The spectrum is shown in Fig. 6 alongside CVPT6 predictions in this spectral region. The former peak can be identified as $\nu_5 + \nu_6$, which is shifted toward higher energies upon C–H deuteration, as expected from the sum of fundamentals. The second last and most intense band is identified as $2\nu_6$. According to the CVPT results, this state has the largest CI overlap with ν_2 (cf. Table III) and therefore is expected to gain the most intensity via Fermi resonance mixing. Moreover, from the data in Table IV, we observe that if one uses the difference between the CVPT6 and experimental fundamental values for ν_6 to adjust the CVPT6 energy of the overtone, PES-2016 transitions yield $2282.2-2 \times (2.4) = 2277.4$ cm^{-1}. The similarly calculated value for the PES-2018 is $2272.3 + 2 \times (3.1) = 2278.5$ cm^{-1}, both being in excellent agreement with experiment. The two signals in the vicinity of $2\nu_6$ can then straightforwardly be assigned to $\nu_4 + \nu_5$ (2271 cm^{-1}) and $4\nu_9$ (2290 cm^{-1}) as only a' states within ±50 cm^{-1} (Fig. 6). The calculations allow two possible assignments for the remaining signal at 2342 cm^{-1}; $\nu_3 + \nu_7$ or $\nu_6 + 2\nu_9$. Due to the strong resonance between ν_3 and $2\nu_8$ in C-deuterated formic acid, combination bands in the Raman spectrum associated with this polyad are always observed as doublets (cf. Table IV). The absence of a second signal therefore rules out $\nu_3 + \nu_7$ as possible assignment. In this context, we note that the Raman band center for $2\nu_6$ (2277 cm^{-1}) significantly deviates from the high-resolution IR value reported by Tan *et al.* (2254.24 cm^{-1}).[71] A likely explanation is the missing Fermi resonance coupling between ν_2 and $2\nu_6$, as Tan *et al.* included only Coriolis-type coupling in the effective fit Hamiltonian (cf. Ref. 71).

With $\nu_6 + 2\nu_9$ assigned to 2342 cm^{-1} and $4\nu_9$ to 2290 cm^{-1} for DCOOH, we are now able to assign the remaining HCOOH Raman signals at 2336 cm^{-1}, 2301 cm^{-1}, and 2298 cm^{-1}. We assign the higher energy band to $\nu_6 + 2\nu_9$ and the two remaining bands to $4\nu_9$ and $\nu_7 + \nu_8 + \nu_9$—the order depending on whether the band observed by Freytes *et al.* at 2338 cm^{-1} corresponds to the Raman band at 2336 cm^{-1} or is indeed $\nu_5 + \nu_8$. Since ν_6 has a very strong IR oscillator strength,[72] it seems plausible that combination bands involving ν_6 are not completely "dark" states, as $2\nu_6$, $\nu_6 + \nu_8$, and $\nu_5 + \nu_6$ are all observed by Freytes *et al.* (cf. experimental intensities reported in Table II of Ref. 7). It is therefore more convincing to assign the two IR bands at 2338 cm^{-1} and 2298.6 cm^{-1} to $\nu_6 + 2\nu_9$ and $4\nu_9$, respectively. The resulting deviation of −2 cm^{-1} (2338 cm^{-1} IR to 2336 cm^{-1} Raman) in turn corroborates the assignment of the Raman signal at 2298 cm^{-1} to $4\nu_9$.

A second although experimentally less certain indication for discrepancies between ICPH and CVPT/MCTDH predictions for higher excited torsional *trans* states comes from a blue-shifted hot band of the ν_3 fundamental of *trans*-HCOOH. We observe four distinct peaks at 1783 cm^{-1}, 1770 cm^{-1}, 1763 cm^{-1}, and 1757 cm^{-1}, which are shifted by +7 cm^{-1}, −6 cm^{-1}, −13 cm^{-1}, and −19 cm^{-1}

relative to the ν_3 fundamental at 1776 cm^{-1} (see Fig. S9 of the supplementary material). Increased intensity between 1770 cm^{-1} and 1776 cm^{-1} indicates other hot contributions where no Q branch can be identified due to the spectral congestion. Focusing first to the down-shifted hot bands, Meyer and Suhm assigned the hot band at 1770 cm^{-1} to $\nu_3 + \nu_7 - \nu_7$, which is consistent with our assignment of $\nu_3 + \nu_7$ to 2395 cm^{-1}.[11] We assign the weakest band shifted by −19 cm^{-1} to $2\nu_3 - \nu_3$, in agreement with $2\nu_3$ band centers from FTIR jet[63] and helium nanodroplet[73,74] measurements and anharmonic calculations that predict a large redshift of 17 cm^{-1}–21 cm^{-1}. Meyer and Suhm were not able to assign the blue-shifted hot band since all DFT VPT2 anharmonicity constants $x_{3,j}$ were negative, predicting exclusively redshifts. Upon O-D isotopic substitution (Fig. S9), we no longer observe a blue-shifted hot band of ν_3. This absence could be an indication of a Fermi resonance between a dark state (involving O–H motion) and a combination state involving ν_3, based on our previous discussion of a blue-shifted hot band of ν_6 in the Raman spectrum of DCOOH. The ICPH and CVPT calculations on PES-2016 indeed predict strong mixing between $\nu_3 + \nu_7$ and $\nu_5 + \nu_6$. Since an experimental band center is available for $\nu_5 + \nu_6$, we can directly compute the hot transition $\nu_5 + \nu_6 - \nu_7$, which is shifted by −3 cm^{-1} and can therefore not explain the observed blue-shifted band. The MCTDH calculation predicts strong mixing between $\nu_7 + 3\nu_9$ and $\nu_3 + \nu_9$, as does CVPT6 on both surfaces. CVPT6/PES-2016 predicts $\nu_4 + \nu_8$ to be involved in this resonance most likely due to the higher energy associated with ν_3. The CI coefficients do not allow us to unambiguously assign $\nu_3 + \nu_9$ and $\nu_7 + 3\nu_9$, and we therefore refer to them as "higher" and "lower" energy state. We obtain predicted shifts of +(3–5) cm^{-1} and −(4–7) cm^{-1} for hot transitions originating from ν_9 into the higher and lower energy state, respectively. The blue-shifted prediction is therefore compatible with the experimental data where the lower energy hot band could be assigned to the increased intensity between 1776 cm^{-1} and 1770 cm^{-1}. This mixing is not predicted by the ICPH calculation, which predicts shifts of +27 cm^{-1} and 0 cm^{-1}.

The previously discussed assignments concerning $4\nu_9$ and possibly $\nu_7 + 3\nu_9$ illustrate the difficulty of high level variational calculations that explicitly take into account wavefunction delocalization effects associated with the necessity to converge more and higher energy eigenvalues compared to single-reference methods.[16,75] In the unified treatment of *cis*- and *trans*-formic acid in the ICPH model, *cis* states correspond to higher (torsional) excitations of the global minimum *trans* isomer. In that treatment, $4\nu_9$ of *trans* corresponds to $n\nu_9$ with $n = 6$, as $n = 4, 5$ correspond to the ground and torsionally first excited state of *cis*-HCOOH.[16] In light of the not fully converged *cis* fundamentals discussed in Sec. III B, it appears plausible that the ICPH eigenstates for $4\nu_9$ and $\nu_7 + 3\nu_9$ are not fully converged either—mind that the eigenvalues are *above*, not below the experimental value—and extension of the vibrational basis set is expected to converge these higher excited torsional ICPH eigenvalues toward experiment.

C. Formic acid spectrum between 2500 cm^{-1} and 3200 cm^{-1}

The assignment of the band at 2504 cm^{-1} is particularly interesting as it was previously reassigned to the nearly degenerate Fermi doublet $2\nu_5/\nu_5 + 2\nu_9$, which is predicted around 2500 cm^{-1} and 2600 cm^{-1}. In this spectral window, Freytes *et al.* reported two bands at 2504 cm^{-1} and 2600 cm^{-1}, respectively.[7] In the Raman jet spectra, we observe a very weak signal at 2504 cm^{-1}, which nicely matches the value reported by Freytes *et al.*, nothing around 2600 cm^{-1}, and then again a band at 2678 cm^{-1} (Figs. S5 and S6 in the supplementary material). With the aid of the anharmonic calculations, the HCOOH peak at 2678 cm^{-1} can unambiguously be assigned to $\nu_4 + \nu_5$ (Table III). Its resonance partner, $\nu_4 + 2\nu_9$, is also predicted around 2600 cm^{-1}, complicating the assignment of the IR band at 2600 cm^{-1}.

In order to get a better understanding of these couplings, we examine the CVPT6 results in more detail. Inspection of the CVPT6 Hamiltonian in this energetic region reveals an interesting situation of different $\nu_5/2\nu_9$ polyads intersecting that we now explore. The presence of significant mixing between states sharing the polyad quantum number $N_p = n_5 + n_9/2$, which has previously been analyzed for $N_p = 1$,[12,16,17] makes it challenging to identify additional resonant interactions between zero-order states. One way to circumvent this issue is to examine the couplings in the polyad eigenstate representation. To obtain this representation, we subsume into the zero-order CVPT6 effective Hamiltonian all the couplings between states sharing common $\{n_1, \ldots, n_4, n_6, \ldots, n_8, N_p\}$ quantum numbers. The Hamiltonian matrix of select states in this representation, which is shown in the supplementary material, is visualized in Fig. 7. The states are labeled with $\{n_4, n_6, N_p\}$ quantum numbers; the blue points correspond to $N_p = 2$, the red and green points correspond to $N_p = 1$, and the remaining states have $N_p = 0$. The y-axis represents the energy difference between the polyad eigenvalues and either those of the 10 × 10 matrix or the fully coupled CVPT6 eigenvalues. The smaller this distance, the better the polyad representation. States within each set of common quantum numbers, i.e.,

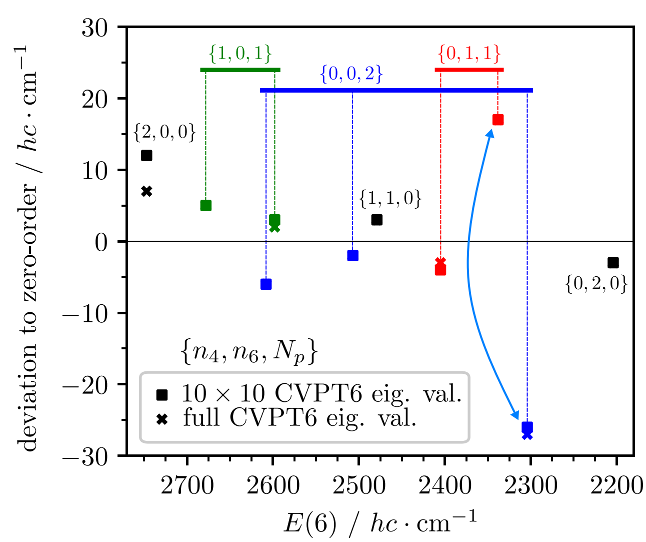

FIG. 7. Eigenvalue differences between the O–H bend/torsion polyad Hamiltonian and both the fully coupled 10-state Hamiltonian (squares) and the full CVPT6 Hamiltonian (crosses) plotted against the full CVPT6 energy for *trans*-HCOOH. The states of the 10-state Hamiltonian satisfy the condition $n_4 + n_6 + N_p = 2$, where $N_p = n_5 + n_9/2$ is the O–H bend/torsion polyad.

{1, 0, 1}, {0, 1, 1}, and {0, 0, 2}, are uncoupled due to the choice of the zero-order Hamiltonian.

There are three important results of this representation. First, the diagonal elements of the matrix match reasonably well with the eigenvalues of the 10 × 10 matrix, with only two exceptions. The exceptions, indicated by the double headed arrow, result from an isolated resonance between the lowest energy states of the blue and red polyads. The cubic terms responsible for this interaction are the same as those that couple $2\nu_9$ to ν_6 in the original normal mode representation that was discussed earlier. We conclude that the current representation is an excellent basis for describing the coupling. Second, although not shown, we note that the interpolyad couplings are substantially different from those of the original harmonic oscillator representation. Finally, the similarities (±1 cm^{-1}) between CVPT6 eigenvalues of the full and effective 10 × 10 Hamiltonian indicate that there is only minor coupling between the states shown here and all other states. There is one exception: the C–H bending overtone $2\nu_4$ ({2, 0, 0}) is missing contributions from the C–H stretch (ν_2). Upon inclusion of ν_2 into the effective Hamiltonian, the {2, 0, 0} eigenvalue agrees to within 1 cm^{-1} with the CVPT6 value.

Beside $2\nu_4$, there are other nearby states that seem to interact with ν_2, as reflected in the CI coefficients of CVPT6 states. We now turn our attention to those peaks. In the vicinity of ±300 cm^{-1} around the ν_2 band center, we observe overall five peaks corresponding to cold formic acid monomer (Fig. 8, top). Based on symmetry information (all a') and the calculated anharmonic energies, the assignments are straightforward (cf. Table II). It is instructive to return to the bright state picture, which offers a more intuitive explanation for the peak structure in the C–H stretching spectrum. The computed CVPT6/PES-2016 eigenvalues plotted alongside the spectrum in Fig. 8 show that all observed *trans* peaks correspond to eigenstates with significant contributions from ν_2. The bright state model further predicts three more Raman signals to be observable, which are anticipated at 2934 cm^{-1} ($2\nu_7 + \nu_8 + \nu_9$), 2934 cm^{-1} ($\nu_6 + \nu_7 + 2\nu_9$), and 2964 cm^{-1} ($\nu_7 + 4\nu_9$). These states interact strongly among each other and one can easily recognize their connection to the interacting states $\nu_7 + \nu_8 + \nu_9$, $\nu_6 + 2\nu_9$, and $4\nu_9$ of a similar polyad, which was discussed in Sec. IV B. Meyer was able to show that two peaks at 2960 cm^{-1} and 2928 cm^{-1} are hidden underneath the rotational contour of ν_2, which she could completely remove by subtracting two Raman spectra with different incident laser polarizations from each other (Fig. 8, bottom).[44] Since ν_2 of $H^{13}COOH$ is shifted down by 11.3 cm^{-1} in the gas phase,[23] the latter peak can most likely be assigned to the ^{13}C isotopolog, whereas $2\nu_7 + \nu_8 + \nu_9$ and $\nu_6 + \nu_7 + 2\nu_9$ are probably hidden under nearby hot bands. As the only a' symmetric state between 2940 cm^{-1} and 2980 cm^{-1} (Table III), we assign the Raman signal at 2960 cm^{-1} to $\nu_7 + 4\nu_9$.

There is evidence in the Raman jet spectrum of DCOOH for a similar combination band involving $4\nu_9$. At 3352 cm^{-1}, 3404 cm^{-1}, and 3421 cm^{-1}, three peaks are observed, corresponding to cold monomer transitions (Fig. S2). Depolarized measurements reveal the former to be a totally symmetric transition. The overall weak intensity of the latter two does not allow any conclusions; however, it seems plausible to assume the same as we have no evidence of any observable a'' symmetric combination or overtone peak in the Raman jet spectrum of any isotopolog. The CVPT6 calculations allow two different assignments of the signal at 3352 cm^{-1}; $\nu_2 + \nu_6$ or $\nu_3 + \nu_4 + \nu_7$. The former assignment seems more plausible, as $\nu_2 + \nu_6$ is predicted to significantly mix with $\nu_6 + 4\nu_9$ and $3\nu_6$, which are predicted at 3352 cm^{-1}, 3408 cm^{-1}, and 3424 cm^{-1}, respectively, accounting for the other two weak peaks observed at 3404 cm^{-1} and 3421 cm^{-1}.

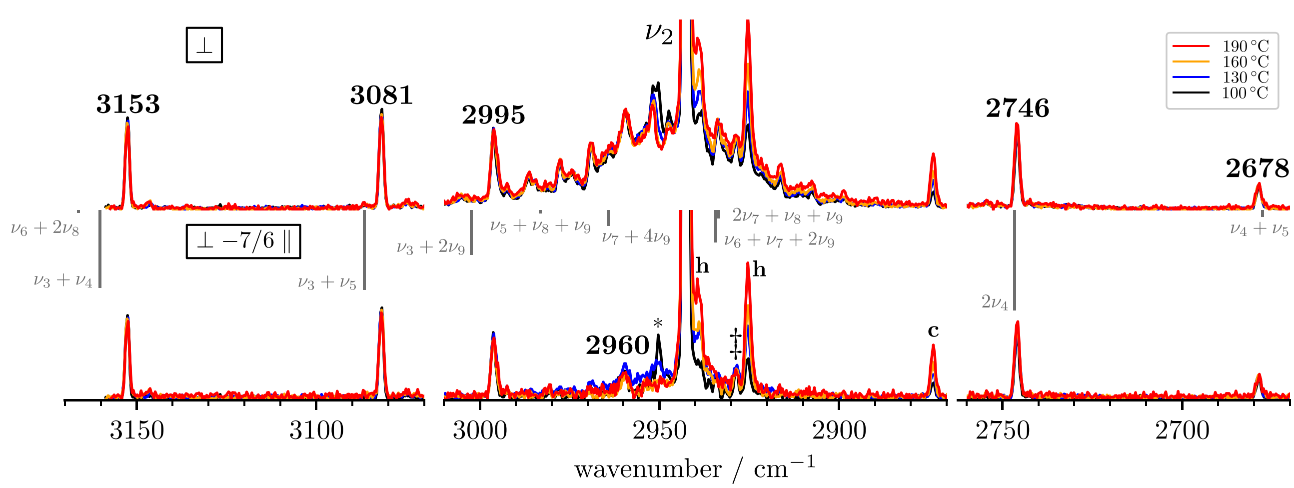

FIG. 8. Raman jet spectrum of HCOOH in helium (<0.1%) between 2670 cm^{-1} and 3170 cm^{-1} with the incident laser polarization perpendicular with respect to the scattering plane (⊥, top) and residual after subtracting 7/6 of the spectrum obtained with polarization parallel to the scattering plane (⊥−7/6‖, bottom). No peaks are observed in omitted intermediate wavenumber intervals (cf. full spectral range in the supplementary material). The spectra are intensity-scaled to ν_2 of *trans*-HCOOH with the lowest intensity among all temperatures. Clusters are marked with an asterisk, and non-isomeric and isomeric, i.e., *cis*, hot bands are labeled "h" and "c," respectively. Isotopic impurities are marked with a double dagger (‡). CVPT6/PES-2016 predictions are shown as gray lines, scaled by the squared contributions from ν_2 to the respective eigenstate, and states with zero overlap are therefore not visible. The spectra were partly shown in Fig. 4.8 of Ref. 44 and are kindly provided by the author.

In light of the newly assigned bands, such as $4\nu_9$, $\nu_6 + 2\nu_9$, and $\nu_5 + 2\nu_9/2\nu_5$ paired with mixing coefficients from CVPT calculations, a consistent picture emerges, which indicates that, while the interaction between ν_5 and $2\nu_9$ remains strong, additional coupling to ν_6 becomes pronounced above 2200 cm^{-1} and beyond. The available experimental data for torsional states of *trans*-formic acid are graphically summarized in Fig. 9. The clumps of nearly degenerate states that are observed in this figure, and that are most evident for *trans*-DCOOD, are conveniently described as nearly degenerate zero-order coupled states known as polyads.

D. Formic acid IR spectrum between 3000 cm^{-1} and 4000 cm^{-1}

Before separately discussing the O–H stretching spectrum of formic acid, we finally review five IR assignments of *trans*-HCOOH concerning bands at 3057 cm^{-1}, 3106.5 cm^{-1}, 3275 cm^{-1}, 3826 cm^{-1}, and 3963.6 cm^{-1} previously reported by Freytes *et al.*[7]

The former two bands are only tentatively assigned by Tew and Mizukami to $\nu_4 + \nu_8 + \nu_9$ (a'') and $\nu_4 + \nu_6 + \nu_7$ (a'), respectively.[16] In light of all four anharmonic calculations, these assignments are plausible. However, in each case, there is a state of the opposite symmetry that seems equally plausible in terms of energetic matching. Neither band is observed in the Raman jet spectrum of HCOOH, which would otherwise help resolve both assignments with additional depolarization information.

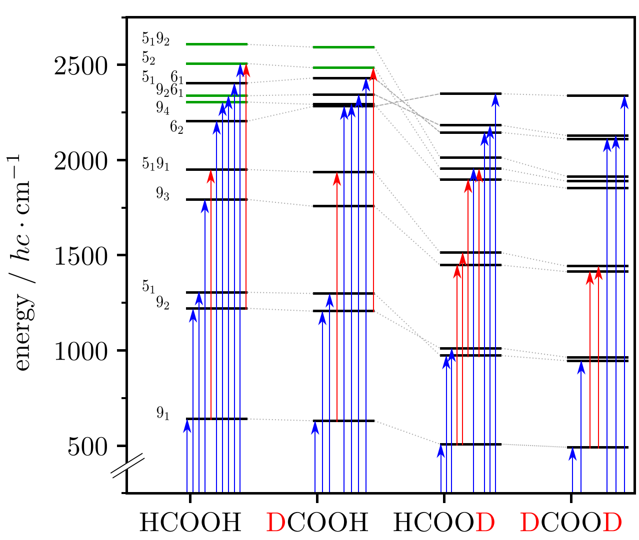

FIG. 9. Energy levels (relative to the ground state) of the O–H/D torsion $n\nu_9$ up to and including n = 4 for all four H/D isotopologs of *trans*-formic acid computed using CVPT6 on PES-2016. As previously discussed (Fig. 7), states above 2200 cm^{-1} are strongly coupled via the O–H torsion. Pairs of energy levels where the CI coefficients do not allow for a one-to-one mapping are highlighted in green. Arrows mark transitions that have been observed in gas phase and jet studies by Raman and IR spectroscopy (this work and compiled from the literature[4,7,9,34,40,41,61]), discriminating between cold transitions (blue), i.e., from the vibrational ground state, and hot transitions from vibrationally excited states (red).

The assignment by Freytes *et al.* regarding the band at 3275 cm^{-1} ($3\nu_6$) was tentatively adopted by Tew and Mizukami. From the perspective of the anharmonic calculations, this assignment is plausible but not unambiguous. There are several other nearby states with 4–6 quanta of excitation. However, in light of the high IR activity of the C–O stretch ν_6 and the apparent variety of observed IR combination/overtone bands that correspond to vibrations associated with C–O stretching motion (cf. Table II), this assignment seems more plausible than any alternative, so we retain it as tentative.

Freytes *et al.* reported an IR band at 3826 cm^{-1}, which they tentatively assigned to $2\nu_4 + \nu_6$.[7] Tew and Mizukami adopted this tentative assignment, and it was not further discussed by Richter and Carbonnière.[16,17] On the basis of the ICPH and CVPT6 calculations, two assignments seem plausible: $2\nu_4 + \nu_6$ and $\nu_3 + 2\nu_8$. These states are even isoenergetic in one of the calculations (Table II). Taking into account the expected error progression, however, $2\nu_4 + \nu_6$ is expected at slightly higher energies 3831 cm^{-1}–3835 cm^{-1}, whereas $\nu_3 + 2\nu_8$ is uniformly expected at 3826 cm^{-1}–3827 cm^{-1}—in excellent agreement with the observed 3826 cm^{-1}.

The last reassignment concerns the band observed at 3963.6 cm^{-1}.[7] Freytes *et al.* originally assigned it to $\nu_2 + \nu_8$, which Tew and Mizukami tentatively adopted.[16] As before, this assignment can be checked by comparing it to hot bands that involve this state. Meyer and Suhm assigned a hot band in the Raman jet spectrum of HCOOH at 2925 cm^{-1} to $\nu_2 + \nu_8 - \nu_8$ (cf. Fig. 8) based on intensity arguments from the expected Boltzmann population of ν_8 and off-diagonal anharmonicity constants from DFT VPT2 calculations.[11] Their assignment is a much better match with the available anharmonic calculations. Using the literature value for ν_8 (1033.47 cm^{-1} from Ref. 7), we obtain a band center for $\nu_2 + \nu_8$ at 3958 cm^{-1}, which nicely matches the error-corrected predictions between 3955 cm^{-1} and 3958 cm^{-1}. Table III shows that for the band at 3963.6 cm^{-1}, two assignments are possible; $\nu_3 + 2\nu_6$ and a member of a set of strongly interacting states, including ν_4, ν_5, ν_7, and ν_9. In analogy to the previous discussion regarding $3\nu_6$, we tentatively assign the band to $\nu_3 + 2\nu_6$, as both CO stretches are the two most IR active fundamentals of formic acid.[7]

E. The O–H stretching spectrum

Complex vibrational spectra of carboxylic acids in the O–H stretching range are usually associated with their cyclic dimers that form two nearly unstrained O–H⋯O hydrogen bonds[76,77] and not their monomers. However, even for monomeric HCOOH, perturbations by skeletal modes seem to complicate the interpretation of the O–H stretching fundamental (ν_1). This complexity lead Hurtmans *et al.* to postpone the ro-vibrational analysis of the high-resolution gas phase spectrum of ν_1, which "is extremely dense."[6] Shortly after, in 2002, Madeja *et al.* used helium nanodroplets to obtain rotationally resolved spectra of the ν_1 band. For *trans*-HCOOH, they observed perturbations of ν_1 and reported three vibrational band centers at 3566.35 cm^{-1}, 3568.63 cm^{-1}, and 3570.66 cm^{-1}. They attributed the presence of the two additional bands as being due to Fermi and Coriolis interactions with $\nu_2 + \nu_7$ and $\nu_2 + \nu_9$.[73] Freytes *et al.* suggested resonance interactions of ν_1 as a likely explanation for a higher density of ro-vibrational lines but overall less than the expected intensity in their room temperature IR spectra, noting similarities between the gas phase and helium nanodroplet spectrum.[7] Two decades later, the ν_1 gas phase high-resolution spectrum of HCOOH remains unanalyzed, to the best of our knowledge.

The Raman scattering spectrum of HCOOH, in constrast to the low-resolution FTIR jet spectrum shown alongside the Raman jet spectrum in Fig. 10, is spectrally less congested and allows the discrimination between different HCOOH bands via their respective Q branches at 3570 cm^{-1}, 3567 cm^{-1}, and 3559 cm^{-1} with an intensity ratio of 20:13:2 and a fourth much weaker band at 3609 cm^{-1}.[40] ν_1 can be assigned to 3570 cm^{-1}, in agreement with the literature value.[7] The excerpt of the CVPT/PES-2016 eigenvalues in Table III shows that the density of states in this spectral region is considerably large, making assignments purely based on the anharmonic predictions very difficult for the other bands. Depolarized spectra [Fig. 10, traces 1(b) and 1(c)] reveal that all three satellites are totally symmetric and C –D substitution [Fig. 10, trace 2(a)] further shows that of these three bands, two persist with only modest shifts of −2 cm^{-1} (3609 cm^{-1} HCOOH to 3607 cm^{-1} DCOOH) and +4 cm^{-1} (3559 cm^{-1} HCOOH to 3563 cm^{-1} DCOOH). The band at 3567 cm^{-1}, which is sensitive to C-D isotopic substitution, can then straightforwardly be assigned to $\nu_2 + \nu_7$. The high intensity of two-thirds of ν_1 suggests possible intensity stealing via Fermi resonance interaction, which in any case can only be of modest strength due to the small shift of −3 cm^{-1} relative to ν_1; in the simplistic picture of a two level interaction, the magnitude of the off-diagonal coupling parameter represents the lower limit of the observed shift. Significant intrinsic oscillator strength can be ruled out; otherwise, $\nu_2 + \nu_7$ would be observed in the HCOOD spectrum, which is not the case (cf. Figs. S1 and S2 in the supplementary material). While the CI coefficients in all four calculations do not suggest significant resonance mixing between $\nu_2 + \nu_7$ and ν_1, only slight modifications to the O–H stretching harmonic force constant to reproduce the experimental value show that this resonance is very sensitive to the energy of the O–H stretch and we obtain mixing ratios of ~50%:50% and a shift of −2 cm^{-1}, using CVPT6 on PES-2016.

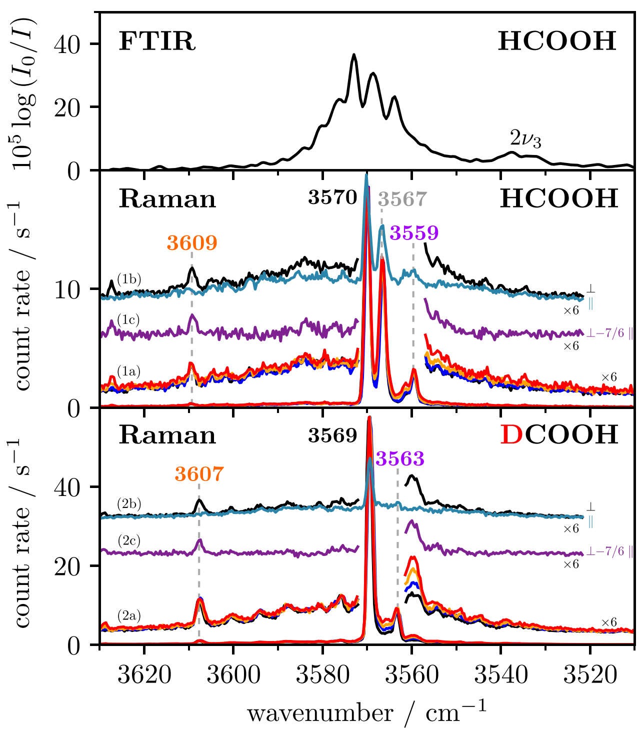

FIG. 10. Low-resolution FTIR jet spectrum of HCOOH in helium (0.04%) and Raman jet spectra of HCOOH and DCOOH in helium (<0.2%–0.3% and <0.4%, respectively) between 3510 cm^{-1} and 3630 cm^{-1}. (a) Raman spectra of a temperature series (100 °C black, 130 °C blue, 160 °C orange, and 190 °C red) are intensity-scaled to ν_1 with the lowest intensity among the four nozzle temperatures. (b) Raman spectra where the incident laser polarization is perpendicular (⊥, default in all other measurements) or parallel (∥) with respect to the scattering plane and (c) residual after subtracting 7/6× ∥ from ⊥ to remove the rotational contour.[67] The FTIR spectrum previously shown in Fig. 4(b) of Ref. 63 was kindly provided by the authors. Due to differing selection rules, the band shape of ν_1 is distinctly different in the Raman (dominant Q branch) and IR spectrum (cf. high-resolution IR spectrum of ν_1 in Fig. 3 of Ref. 6).

The currently available calculations do not allow us to unambiguously assign the other two satellites at 3609 cm^{-1} and 3559 cm^{-1}. Experimentally, we can narrow down the list of possible resonance partners: Isotopic C-D substitution excludes the C–H stretch, in-plane bending, and out-of-plane bending vibrations ν_2, ν_4, and ν_8. The very strong Fermi resonance between the C=O stretch ν_3 and $2\nu_8$ in DCOOH also makes ν_3 an unlikely candidate. Depolarized spectra shown in Fig. 10 further exclude odd quantum numbers for the torsion $n\nu_9$, as all satellites are totally symmetric. We therefore conclude that these satellites correspond to a member of the interacting states ν_5, ν_6, $2\nu_7$, and $2\nu_9$, which seem to be strongly coupled in this energetic regime, as can readily be seen by inspection of the CI coefficients reported in Table III and the supplementary material to Ref. 16.

As expected, O–H deuteration detunes these resonance perturbations of ν_1 and we only observe one peak for *trans*-HCOOD and *trans*-DCOOD, which agree within 1 cm^{-1} with high-resolution values reported in the literature.[37,78] For DCOOD, Goh *et al.* observed small perturbations of ro-vibrational lines with a high K value that were too weak to be analyzed.[78] For HCOOD, A'dawiah *et al.* observed slight perturbations of ν_1, which they ascribed to Coriolis interactions with $3\nu_7 + \nu_8$.[37] By using an effective fit Hamiltonian, they obtained a band center at 2601.13 cm^{-1} for the perturbing level. Our CVPT calculations disagree with this assignment, as $3\nu_7 + \nu_8$ is predicted to be significantly higher in energy around 2700 cm^{-1}. The best energy match by far is $\nu_7 + \nu_8 + 2\nu_9$, which is predicted between 2589 cm^{-1} and 2604 cm^{-1} (Tables III and IV).

V. COMPARISON OF FORMIC ACID POTENTIALS

Using experimental data from the literature and newly assigned in this work, Fig. 4 can be extended beyond fundamentals and their strong resonance partners. Using the same vibrational framework (CVPT), the performance of PES-2016 and PES-2018 is compared for 155 energy levels in Fig. 11, including the three deuterated isotopologs. Similar to the conclusions drawn in Secs. III and IV, it can be seen that PES-2016 almost exclusively overestimates and PES-2018 often underestimates the energy. The experiment is in

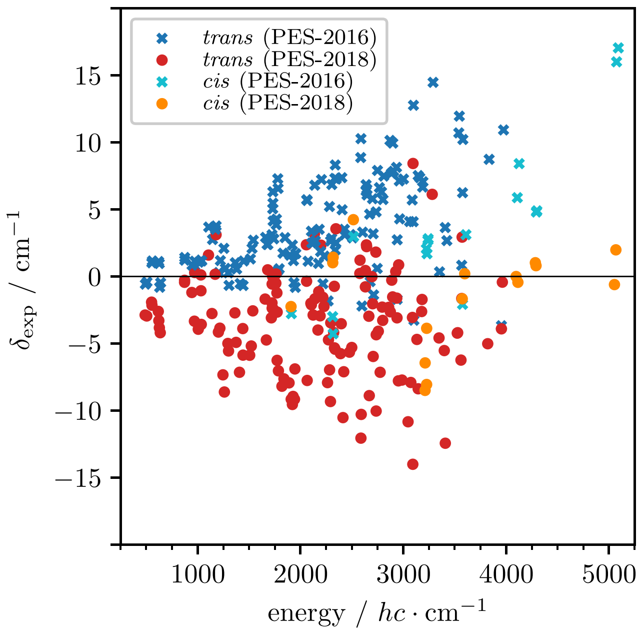

FIG. 11. Deviation between 155 experimental and CVPT6 energy levels ($\delta_{\text{exp}} = \tilde{\nu}_{\text{calc}} - \tilde{\nu}_{\text{exp}}$) of formic acid against the predicted energy (relative to the vibrational ground state of the *trans* isotopolog). Data for all four H/D isotopologs are shown in Tables II and IV for *trans*- and Table S3 (supplementary material) for *cis*-formic acid. The 2376 cm^{-1} band of HCOOH (Table II) is omitted.

many cases (halfway) between both, which is also exemplified in Fig. 6. These discrepancies between both PESs seem surprising at first sight, as the underlying *ab initio* methods are of similar quality.

To highlight the role of anharmonic effects, we return to the second order result of Eq. (1) and focus on the $x_{i,i}/x_{i,j}$ values. One can extract these values experimentally using select high-resolution or jet-cooled combination or overtone transitions and compare them to values obtained using the same transition energies calculated with CVPT6. It is more instructive, however, to compare to $x_{i,i}/x_{i,j}$ values obtained with second order perturbation theory. These values are familiar to workers in the field and allow for a global comparison of anharmonic effects with 45 parameters. In contrast, the CVPT6 Hamiltonian has over 4000 terms. Before we make these comparisons, we note that the differences between the two theoretical results arise through resonance effects and higher order perturbative contributions. Even at the second order, with the equivalent treatment of resonances, one will find differences between curvilinear and rectilinear normal mode representations of the $x_{i,i}/x_{i,j}$ values.[48]

We report the full **x** matrices for both PESs computed with CVPT2 in the supplementary material for *cis*- and *trans*-HCOOH (Table S5). The values of these terms depend on the resonance terms included in the CVPT transformations, but the same resonant terms are present for both potential surfaces. In comparing these values, we first focus on the C=O stretching degree of freedom ν_3, since there are notable differences in the fundamental values (cf. Table I). Comparing the PES-2016 and PES-2018 CVPT6 results, we find 1821 cm^{-1} and 1810 cm^{-1}, respectively, for the *cis* isomer and 1783 cm^{-1} and 1773 cm^{-1}, respectively, for the *trans* isomer. Inspection of individual anharmonicity constants $x_{3,i}$, obtained directly with CVPT2, reveals maximum absolute deviations of 2 cm^{-1} for *trans* but 7 cm^{-1} for *cis*-HCOOH. More generally, the anharmonic terms for *trans*-formic acid are similar for the two surfaces, and the resulting deviations in anharmonic energy levels can primarily be ascribed to deviations in the underlying harmonic potential. The argument holds when comparisons are made to experimentally extracted[63] $x_{1,j}$ values for ν_1 of *trans*-HCOOH (see Table S6). For *cis*-formic acid, the differences between the surfaces in both $x_{i,j}$ values and harmonic values are more pronounced. In several instances, these differences tend to cancel to yield similar fundamental transitions (Table I).

Finally, we turn to the large-amplitude O–H torsion that connects the two conformational isomers. In the energetic regime so far experimentally explored, diagonal anharmonic contributions and resonance couplings are equally well captured by both surfaces. This is elucidated in Fig. 12 where the energetic differences between subsequent energy levels in the *trans* well are compared. Deviations between higher and lower orders of perturbation theory (CVPT6 vs CVPT2) and anharmonic contributions from both surfaces (CVPT6 on PES-2016 vs PES-2018) appear to become substantial starting with $5\nu_9$. Delocalization effects between the *cis* and *trans* well are expected to start with $6\nu_9$.[16] The precise energy of $6\nu_9$ should be a sensitive marker for high level calculations due to additional wavefunction mixing with the *cis* well and anharmonic potential contributions close to the isomerization threshold.

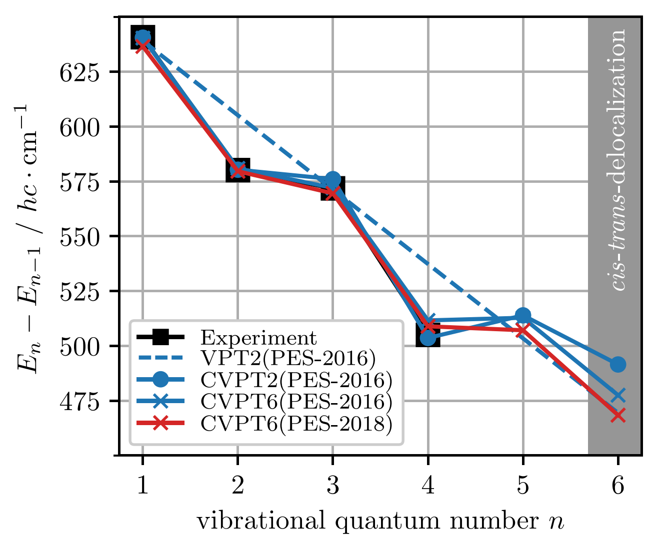

FIG. 12. Energy differences between subsequent torsional states of *trans*-HCOOH as a function of the vibrational quantum number *n* where zero corresponds to the ground state. The VPT2 energies, which are equivalent to CVPT2 without resonances, are computed according to Eq. (1) using the harmonic wavenumber $\tilde{\omega}_9$ and deperturbed diagonal anharmonicity constant $x^*_{9,9}$; the slope equals $2x^*_{9,9}$. Delocalization effects between the *cis* and *trans* wells are expected to start with $n = 6$.[16]

VI. CONCLUSIONS

Utilizing the previously published CCSD(T)-F12 quality potential energy surfaces of formic acid in conjunction with high order canonical Van Vleck perturbation theory, we have revisited the IR and Raman spectra of monomeric *trans*-formic acid and its three deuterated isotopologs. Overall, we were able to add 11 new vibrational band centers of *trans*-HCOOH to the database and reassign seven previous IR assignments. We also assigned 53 new vibrational band centers of deuterated *trans* isotopologs that significantly extend the database, which until now was mostly composed of fundamentals.

Three strategies were pursued in making these assignments. In the absence of anharmonic Raman intensities, the simple model of dark states gaining intensity via resonance mixing with nearby fundamentals proved successful in providing a qualitative explanation for a plethora of (un)observed combination and overtone peaks in the Raman jet spectra of formic acid monomer. Using temperature as a population control, we have identified many hot bands and, in selected cases, used them to critically review other assignments. These bands allow direct insights into the anharmonic contributions to the Hamiltonian. Still many more observed hot bands remain unassigned, and a future direction is to incorporate the calculation of Raman activities into the CVPT6 framework. We have also made use of multiple isotopologs to probe the quality of the potential surface to aid in peak assignments. The approach included identifying bands in the Raman spectra that correspond to the two CO stretching vibrations (ν_3 and ν_6) of naturally occurring formic acid-^{13}C. The resulting extensive vibrational reference data, particularly highly excited torsional and many resonance coupled states, ultimately will help establish formic acid as a model system to test and evaluate anharmonic vibrational methods for polyatomic molecules.

Comparison between second through sixth order Van Vleck perturbation theory validates the popular approach of second order vibrational perturbation theory with additional resonance treatment for fundamentals and binary combinations/overtones but also shows its limitations for quantitatively predicting highly excited vibrational states beyond two quanta. Errors for three- and four-quantum states were shown to be up to 20 cm^{-1}, even more with the increase in energy and excitation of vibrational quanta. The close experiment-theory interplay revealed increasing deviations of internal coordinate path Hamiltonian eigenvalues to the experiment for highly excited torsional states, further demonstrating the importance of close collaboration between experiment and theory.[79] While the question to this discrepancy remains open, several indications point to unconverged torsional eigenvalues.

As we have discussed and shown in Fig. 9, the large-amplitude O–H torsion leads to interesting and challenging dynamical features of *trans*-formic acid. The data shown in Fig. 9 illustrate how this torsion coupling extends to multiple isotopologs. The strong coupling among states, which share the polyad quantum number $N_p = n_5 + n_9/2$, is present for many of the isotopologs. Moreover, our analysis of these states (see Fig. 7), which shows a breakdown of the polyad quantum number $N_p = n_5 + n_9/2$ for $N_p \geq 2$ due to mixing with the C–O stretch ν_6, extends to *trans*-DCOOH starting with $N_p = 1.5$. The resonance interactions involving the torsion extend to the *cis* well despite its lower frequency, and they are expected for $6\nu_9$,[16] which can be investigated with appropriate methods, such as the internal coordinate path Hamiltonian. This work is intended to help calibrate future endeavors near the isomerization threshold.

Rotationally cold Raman jet spectra of HCOOH and DCOOH allowed us to identify perturbing states via their respective *Q* branches that interact with the O–H stretching fundamental ν_1, leading to a complicated ro-vibrational spectrum.[6] We have presented experimental evidence for the involvement of the aforementioned polyad (possibly including the OCO bend) in this resonance with ν_1. Next steps in understanding the O–H stretching and torsion dynamics include refinement of the existing potential energy surfaces and analysis of the high-resolution spectrum of ν_1, which we strongly encourage. Better understanding of the interaction between O–H stretching and skeletal modes of isolated formic acid is an important stepping stone in elucidating the complex vibrational spectrum of the cyclic formic acid dimer and gaining new physical insight into the dynamics of strongly hydrogen bonded systems. This paves the way for theoretical work revisiting the vibrational spectrum of monomeric formic acid beyond 4000 cm^{-1}, as many of the band centers reported by Freytes *et al.* remain tentative.[7] Further investigation along the lines presented in this work will deepen the understanding of coupling across chemical bonds as resonance mixing between the CH and OH stretches, and short time intramolecular vibration redistribution (IVR) dynamics become significant in the OH overtone spectra of formic acid.[13,64]

SUPPLEMENTARY MATERIAL

See the supplementary material for a full set of computed CVPT eigenvalues for H/D isotopologs of *trans*-formic acid, fundamentals of *cis*-formic acid and *trans*-formic acid-^{13}C, and Raman jet spectra in the spectral range between 870 cm^{-1} and 3750 cm^{-1}.

ACKNOWLEDGMENTS

A.N. gratefully acknowledges funding by the Deutsche Forschungsgemeinschaft (DFG; Project No. 389479699/GRK2455), thanks the Fonds der Chemischen Industrie (FCI) for a generous scholarship, and thanks Katharina A. E. Meyer, Martin A. Suhm, and David P. Tew for valuable discussions. E.L.S. gratefully acknowledges support from the NSF via Grant No. CHE-1900095. The authors thank Falk Richter for kindly supplying *ab initio* harmonic frequencies of *trans*-HCOOH at the CCSD(T)-F12a/aVTZ level.

APPENDIX A: CVPT EIGENSTATES OF *TRANS*-FORMIC ACID

To aid the discussion of *trans*-formic acid band assignments in Sec. IV, we report selected vibrational eigenstates together with squared coefficients of the two leading contributing basis states in Table III.

TABLE III. Vibrational energy levels (in cm^{-1}) and two leading squared coefficients (P) for selected states of different *trans*-formic acid isotopologs (energies relative to the vibrational ground state of the *trans* isotopolog) obtained from PES-2016[16] using CVPTn with n = 2, 4, 6. The energy difference $\Delta(n) = E(n) - E(6)$ is shown for n = 2, 4. Squared coefficients printed as "0.00" are below 0.5%. Eigenstates are numbered (No.) according to the CVPT6 energy, where "1" corresponds to the vibrational ground state. The full set of eigenvalues is reported in the supplementary material (Tables S7–S10).

No.	Γ	$E(6)$	Δ(4)	Δ(2)	P_1	State	P_2	State
trans-HCOOH								
29	a'	2303.8	−0.2	0.3	0.92	$7_18_19_1$	0.03	9_4
30	a'	2304.8	−2.5	−4.5	0.34	9_4	0.32	6_19_2
31	a'	2337.9	0.0	8.0	0.41	9_4	0.28	6_19_2
32	a''	2338.4	0.5	−1.4	0.67	5_18_1	0.30	8_19_2
33	a'	2358.6	−0.9	1.4	0.99	6_17_2	0.01	7_29_2
34	a''	2368.0	−0.5	−0.6	0.93	$6_17_19_1$	0.06	7_19_3
35	a'	2402.4	0.1	−2.1	0.65	3_17_1	0.20	5_16_1
36	a'	2405.0	0.4	0.2	0.43	5_16_1	0.32	3_17_1
37	a''	2415.6	−0.2	0.0	0.52	4_18_1	0.26	3_19_1
38	a''	2418.4	0.0	2.1	0.43	4_18_1	0.23	3_19_1
39	a''	2427.5	0.1	5.0	0.50	3_19_1	0.38	7_19_3
…								
42	a'	2506.9	0.3	−2.0	0.52	5_2	0.31	5_19_2
…								
46	a''	2578.5	1.5	1.2	0.76	$5_17_19_1$	0.17	7_19_3
47	a'	2597.8	−0.5	−1.4	0.60	4_19_2	0.30	4_15_1
48	a'	2607.5	2.4	−0.6	0.42	5_2	0.41	5_19_2
49	a'	2634.4	−0.4	2.9	0.94	4_17_2	0.05	7_29_2
50	a''	2652.7	0.2	5.2	0.91	$4_17_19_1$	0.07	7_19_3
51	a'	2677.6	0.8	5.2	0.57	4_15_1	0.22	4_19_2
52	a'	2692.0	−1.7	−1.8	1.00	7_18_2	0.00	3_17_1
…								
68	a'	2940.3	−0.1	0.5	0.90	2_1	0.03	3_15_1
69	a'	2964.3	0.8	11.5	0.45	7_19_4	0.23	$6_17_19_2$
70	a''	2964.9	0.2	−1.3	0.64	$5_17_18_1$	0.32	$7_18_19_2$
71	a'	2983.2	2.1	0.6	0.76	$5_18_19_1$	0.18	8_19_3
…	(Between 133 and 147 only a' states)							
133	a'	3544.9	0.1	2.7	0.94	3_2	0.02	$3_15_17_1$
135	a'	3564.0	−3.8	−2.6	0.31	$6_17_29_2$	0.18	7_29_4
136	a'	3564.5	−0.7	5.2	0.85	$7_38_19_1$	0.05	$6_17_29_2$
137	a'	3565.2	1.6	1.6	0.66	4_16_2	0.09	5_26_1
138	a'	3567.8	0.0	1.6	0.83	2_17_1	0.03	$3_15_17_1$
140	a'	3576.2	−0.5	−2.8	0.54	1_1	0.13	4_16_2
142	a'	3581.8	1.2	1.3	0.43	1_1	0.14	5_19_4
143	a'	3591.7	1.7	14.2	0.47	7_29_4	0.20	$6_17_29_2$
145	a'	3610.9	2.0	1.0	0.75	$5_17_18_19_1$	0.18	$7_18_19_3$
146	a'	3614.5	−2.6	5.8	0.88	6_17_4	0.03	5_26_1
147	a'	3615.0	6.1	10.2	0.30	5_26_1	0.20	5_19_4
…								
182	a''	3806.9	0.4	7.1	0.67	$3_14_19_1$	0.18	$4_17_19_3$
183	a'	3824.6	−2.5	−0.9	0.60	5_17_4	0.30	7_49_2
184	a'	3834.7	−1.6	−2.8	0.84	3_18_2	0.10	4_26_1
185	a'	3834.8	2.0	1.3	0.72	4_26_1	0.12	3_18_2
186	a''	3840.5	0.7	0.9	0.73	$5_17_39_1$	0.16	7_39_3
…								
205	a'	3934.1	−1.0	5.7	0.50	$4_15_17_2$	0.23	$4_17_29_2$
206	a'	3948.8	−2.5	1.7	0.98	7_38_2	0.01	$7_18_29_2$
207	a''	3950.7	1.6	9.2	0.61	$4_15_17_19_1$	0.12	$4_27_19_1$
208	a''	3954.3	−0.7	−1.7	0.92	2_18_1	0.03	4_28_1

TABLE III. (*Continued.*)

No.	Γ	$E(6)$	Δ(4)	Δ(2)	P_1	State	P_2	State
209	a''	3963.4	−1.9	1.8	0.97	$7_2 8_2 9_1$	0.01	$7_3 8_1 9_2$
210	a'	3965.3	3.0	−3.0	0.53	$4_2 5_1$	0.16	$4_2 9_2$
211	a''	3967.8	−3.4	−6.1	0.42	$6_1 7_1 8_1 9_2$	0.24	$5_1 6_1 7_1 8_1$
212	a'	3974.5	−0.2	0.6	0.94	$3_1 6_2$	0.02	$5_1 6_2 7_1$
213	a'	3977.3	−0.8	6.5	0.31	$4_2 9_2$	0.24	$4_1 5_2$
214	a''	3983.6	1.9	25.0	0.57	$6_2 9_3$	0.21	$5_1 6_2 9_1$
trans-DCOOH								
35	a'	2218.4	0.2	1.0	0.84	2_1	0.04	6_2
36	a''	2225.9	0.2	1.2	1.00	$4_1 7_1 9_1$	0.00	$7_1 9_3$
37	a'	2269.2	−0.2	−1.0	0.68	$4_1 5_1$	0.25	$4_1 9_2$
38	a'	2282.2	0.4	−0.5	0.76	6_2	0.10	9_4
39	a'	2292.6	0.5	2.6	0.58	9_4	0.16	6_2
40	a'	2344.5	−1.1	−1.5	0.60	$6_1 9_2$	0.27	$5_1 6_1$
41	a'	2349.9	−0.6	−0.5	0.50	$7_1 8_2$	0.45	$3_1 7_1$
42	a''	2365.3	−0.2	−0.5	0.51	$3_1 9_1$	0.42	$8_2 9_1$
43	a'	2380.1	−0.7	0.9	0.96	$6_1 7_2$	0.03	$7_1 8_2$
44	a''	2381.5	0.2	1.5	0.51	$6_1 7_1 9_1$	0.34	$7_1 9_3$
45	a'	2384.0	−0.3	1.0	0.51	$3_1 7_1$	0.46	$7_1 8_2$
46	a''	2397.8	−0.1	0.9	0.34	$6_1 7_1 9_1$	0.21	$8_2 9_1$
47	a''	2403.2	−0.2	2.4	0.30	$3_1 9_1$	0.28	$8_2 9_1$
48	a'	2431.1	0.1	−1.2	0.67	$5_1 6_1$	0.28	$6_1 9_2$
49	a'	2454.7	−0.8	0.4	0.67	$7_2 9_2$	0.31	$5_1 7_2$
…								
152	a'	3382.0	−0.3	5.0	0.98	$7_3 8_1 9_1$	0.01	$5_1 7_3$
153	a'	3392.4	−0.1	−2.5	0.64	$4_1 5_1 6_1$	0.19	$4_1 6_1 9_2$
154	a'	3407.6	0.3	4.2	0.48	$6_1 9_4$	0.13	6_3
155	a''	3417.1	2.2	15.7	0.70	$7_1 9_5$	0.16	$5_1 7_1 9_3$
156	a''	3418.7	−1.3	−1.2	0.59	$5_1 7_2 8_1$	0.36	$7_2 8_1 9_2$
157	a'	3423.7	−1.5	−5.5	0.61	6_3	0.14	$6_1 9_4$
158	a'	3424.1	−0.7	0.7	0.61	$4_1 7_2 9_2$	0.29	$4_1 5_1 7_2$
159	a''	3433.0	0.3	0.1	0.99	$4_2 7_1 8_1$	0.00	$4_1 8_2 9_1$
160	a'	3434.9	0.5	2.8	0.62	$5_1 7_1 8_1 9_1$	0.22	$7_1 8_1 9_3$
161	a'	3437.3	−3.0	−7.0	0.44	$3_1 8_2$	0.42	8_4
…	(Between 186 and 202 only a' states)							
186	a'	3542.6	0.6	8.4	0.59	$7_2 9_4$	0.17	$5_1 7_2 9_2$
189	a'	3557.9	0.2	−6.3	0.42	$5_1 6_2$	0.20	$6_2 9_2$
190	a'	3563.0	−0.4	2.0	0.34	$3_1 7_1 9_2$	0.18	$3_1 5_1 7_1$
191	a'	3566.4	2.4	−7.7	0.24	$4_1 5_2$	0.23	$4_1 5_1 9_2$
192	a'	3569.9	0.1	−2.0	0.86	1_1	0.05	$4_1 5_2$
193	a'	3582.1	−1.6	2.7	0.58	$6_1 7_2 9_2$	0.28	$5_1 6_1 7_2$
194	a'	3589.9	−1.2	1.9	0.56	$3_1 7_3$	0.37	$7_3 8_2$
195	a'	3597.8	−0.6	−0.1	0.30	$7_1 8_2 9_2$	0.27	$5_1 7_1 8_2$
198	a'	3607.1	0.0	−1.3	0.76	$4_1 6_1 8_1 9_1$	0.13	$4_1 8_1 9_3$
199	a'	3615.1	−1.5	−3.7	0.45	$5_2 6_1$	0.22	$5_1 6_1 9_2$
201	a'	3620.9	−2.6	3.2	0.97	$6_1 7_4$	0.02	$7_3 8_2$
202	a'	3624.6	−0.6	3.6	0.60	$7_3 8_2$	0.38	$3_1 7_3$
trans-HCOOD								
33	a'	2103.2	−0.6	−0.8	0.72	$7_1 8_1 9_1$	0.25	$5_1 7_2$
34	a'	2134.7	0.8	4.5	0.67	$7_2 9_2$	0.23	$5_1 7_2$
35	a'	2145.0	−0.4	−2.5	0.60	$5_1 6_1$	0.38	$6_1 9_2$
36	a''	2150.6	−0.6	0.6	0.94	$7_2 8_1$	0.06	$7_3 9_1$

TABLE III. (*Continued.*)

No.	Γ	$E(6)$	$\Delta(4)$	$\Delta(2)$	P_1	State	P_2	State
37	a'	2182.3	0.0	0.4	0.58	$6_1 9_2$	0.39	$5_1 6_1$
38	a''	2195.7	−0.5	2.6	0.93	$7_3 9_1$	0.06	$7_2 8_1$
39	a''	2208.5	−0.5	−1.8	0.96	$6_1 8_1$	0.03	$6_1 7_1 9_1$
…								
62	a''	2574.6	−0.1	3.4	0.51	$5_1 7_1 8_1$	0.28	$7_2 9_3$
63	a''	2604.4	−0.1	1.2	0.63	$7_1 8_1 9_2$	0.14	$5_1 7_1 8_1$
64	a''	2614.1	0.1	−1.1	0.67	$6_1 9_3$	0.29	$5_1 6_1 9_1$
65	a'	2618.3	−1.6	−0.9	0.91	$7_1 8_2$	0.08	$7_2 8_1 9_1$
66	a''	2636.1	1.9	7.3	0.55	$5_1 7_2 9_1$	0.33	$7_2 9_3$
67	a'	2637.8	−0.1	−0.5	0.99	1_1	0.01	$3_1 5_1$

APPENDIX B: DEUTERATED *TRANS*-FORMIC ACID DATA

Experimental band centers from this work and the literature are compactly summarized in Table IV for the three deuterated *trans*-formic acid isotopologs.

TABLE IV. Vibrational wavenumbers (in cm^{-1}) of deuterated *trans*-formic acid states. Multi-configuration time-dependent Hartree (MCTDH)[18] and canonical Van Vleck perturbation theory (CVPT) predictions using two different analytical PES[16,17] are shown together with perturbation-free experimental data. The asterisk denotes newly assigned bands, and the dagger denotes a reassignment. Tentative assignments are in brackets, not fully converged MCTDH energies are given in energy ranges (adopted from Ref. 18), and energy levels obtained from hot band assignments are italicized. Numbers in the state labels refer to the vibrational degree of freedom, which is indexed with the respective quanta of excitation.

	State		Exp.		PES-2016[a]	PES-2018[b]	
	Label	Γ	Ra. jet[c]	Lit.	CVPT6	MCTDH	CVPT6
trans-DCOOH							
	7_1	a'	620	620.57[d]	621	617	617
	9_1	a''		631.54[d]	631	628	628
	8_1	a''		873.39[e]	875	872	873
	4_1	a'	971	970.89[e]	971	971	971
	6_1	a'	1142	1142.31[f]	1145	1139	1139
	9_2	a'	1206		1206	1202	1202
	5_1	a'	1299	1297[g]	1299	1294	1294
	$3_1/8_2$	a'	1725	1725.87[h]	1731	1723	1724
	$3_1/8_2$	a'	1762	1762.9[h]	1766	1761	1762
*	$6_1 9_1$	a''	*1779*		1779	1773	1773
*	$7_1 9_2$	a'	1828		1830	1819	1820
*	$5_1 7_1$	a'	1919		1921	1910	1910
*	$5_1 9_1$	a''	*1937*		1937	1928	1928
*	$4_1 6_1$	a'	2103		2106	2101	2101
*	$4_1 9_2$	a'	2174		2175	2170	2170
	2_1	a'	2219	2219.69[i]	2218	2217	2217
*	$4_1 5_1$	a'	2271		2269	2263	2263
	6_2	a'	2277	2254.24[i]	2282	n.r.	2272
*	9_4	a'	2290		2293	2282	2283
*	$6_1 9_2$	a'	2342		2344	n.r.	2337
*	$5_1 6_1$	a'	2428		2431	2421	2421

TABLE IV. (*Continued.*)

	State		Exp.		PES-2016[a]	PES-2018[b]	
	Label	Γ	Ra. jet[c]	Lit.	CVPT6	MCTDH	CVPT6
*	$5_2/5_19_2$	a'	*2482*		2485	2476	2476
	$5_2/5_19_2$	a'			2593	2582	2581
*	$3_18_1/8_3$	a''	*2578*		2588	2576	2579
*	$3_18_1/8_3$	a''	*2641*		2647	2641	2643
*	$3_14_1/4_18_2$	a'	2695		2701	2692	2695
*	$3_14_1/4_18_2$	a'	2731		2736	2730	2733
*	$3_16_1/6_18_2$	a'	2860		2870	n.r.	2858
*	$3_16_1/6_18_2$	a'	2898		2906	n.r.	2896
*	2_16_1	a'	3352		3352	n.r.	3347
*	6_19_4	a'	3404		3408	n.r.	3398
*	6_3	a'	3421		3424	n.r.	3409
	[1_1-Res]	a'	3563				
	1_1	a'	3569	3566[g]	3579	3568	3572
	[1_1-Res]	a'	3607				
trans-HCOOD							
	9_1	a''		508.13[j]	508	505	505
	7_1	a'	558	558.27[j]	559	556	556
	5_1	a'	972	972.85[k]	973	969	969
	9_2	a'	1010	1011.68[k]	1011	1006	1006
	8_1	a''	1031[l]		1032	1029	1031
	6_1	a'	1176	1177.09[m]	1180	1179	1179
	4_1	a'	1365	1366.48[n]	1366	1362	1362
*	9_3	a''	*1447*		1448	1441	1441
*	5_19_1	a''	*1512*		1513	1507	1506
*	5_17_1	a'	1527		1529	n.r.	1522
*	8_19_1	a'	1539		1542	1535	1536
	6_19_1	a''	*1679*	1680.96[o]	1683	1681	1681
	6_17_1	a'	1730	1732.08,[o] 1735.81[p]	1734	1730	1730
	3_1	a'	1772	1772.12[o]	1779	1771	1771
*	9_4	a'	*1897*		1899	1890	1889
*	5_2	a'	1953		1955	1946	1946
*	8_2	a'	2055		2061	2054	2057
*	5_16_1	a'		2142.4[q]	2145	2141	2141
*	6_19_2	a'		2178.8[q]	2182	2178	2178
*	3_17_1	a'	2327		2334	2322	2323
*	6_2	a'	2341		2348	2345	2345
†	$7_18_19_2$	a''		2601.13[r]	2604	2589	2591
	7_38_1	a''			2712	n.r.	2699
	1_1	a'	2631	2631.64[r]	2638	2629	631[r]
	4_2	a'	2713	2714[s]	2712	2706	2707
*	3_15_1	a'	2741		2749	n.r.	2737
*	3_19_2	a'	2782		2788	2734–2775	2775
	2_1	a'	2938	2938.2[s]	2941	2934	2936
	3_16_1	a'	2954		2961	2954	2955
*	$4_16_17_1$	a'	3092		3096	n.r.	3089
*	3_14_1	a'	3137		3145	3131	3132
*	1_17_1	a'	3184		3191	3180	3182
	3_2	a'	3529	3531/3526[t]	3540	n.r.	3525
trans-DCOOD							
	9_1	a''		492.23[u]	492	489	489
	7_1	a'	554	554.44[u]	555	552	552

TABLE IV. (*Continued.*)

	State		Exp.		PES-2016[a]	PES-2018[b]	
	Label	Γ	Ra. jet[c]	Lit.	CVPT6	MCTDH	CVPT6
	8_1	a''		873.2[v]	874	872	873
	5_1	a'	945	945.0[w]	946	944	944
	9_2	a'			964	961	961
	4_1	a'	1039	1042[w]	1040	1035	1035
	6_1	a'	1170	1170.80[x]	1173	1170	1170
*	9_3	a''	*1414*		1413	1407	1407
*	$5_1 9_1$	a''	*1443*		1442	1439	1439
	$3_1/8_2$	a'	1725	1725.12[y]	1730	1722	1723
*	$6_1 9_1$	a''	*1658*		1661	1657	1656
*	$6_1 7_1$	a'	*1720*		1723	1717	1717
	$3_1/8_2$	a'	1761	1760.0[w]	1765	1759	1760
*	4_2	a'	2073		2074	2076	2065
*	$5_1 6_1$	a'	2108		2110	n.r.	2106
*	$6_1 9_2$	a'	2126		2129	2123	2123
	$4_1 6_1$	a'	2194	2195.1[w]	2196	2191	2191
	2_1	a'	2231	2231.8[w]	2233	2228	2229
	6_2	a'	2330	2326.2[w]	2338	2330	2329
*	$3_1 8_1/8_3$	a''	*2577*		2586	2574	2577
	1_1	a'	2632	2631.87[z]	2638	2629	2631
*	$3_1 8_1/8_3$	a''	*2639*		2646	2638	2641
*	$3_1 5_1/5_1 8_2$	a'	2668		2673	n.r.	2665
*	$3_1 5_1/5_1 8_2$	a'	2704		2707	n.r.	2702
*	$3_1 4_1/4_1 8_2$	a'	2761		2768	n.r.	2757
*	$3_1 4_1/4_1 8_2$	a'	2797		2803	2792	2795
*	$3_1 6_1/6_1 8_2$	a'	2888		2898	2887–2925	2888
*	$3_1 6_1/6_1 8_2$	a'	2926		2934	n.r.	2926
*	$2_1 8_1$	a''	*3096*		3099	3092	3094
*	$1_1 7_1$	a'	3181		3188	n.r.	3178

[a]Reference 16.
[b]Reference 18.
[c]Fundamentals and resonance partners from Ref. 40.
[d]Reference 35.
[e]Reference 32.
[f]Reference 80.
[g]Reference 41.
[h]Reference 31.
[i]Reference 71; for the interaction between ν_2 and $2\nu_6$, only Coriolis coupling was included in the model Hamiltonian.
[j]Reference 33.
[k]Reference 34.
[l]Estimated from overtone transition of *trans*-HCOOD and the experimental diagonal anharmonicity constant for *trans*-HCOOH (see Sec. III B for details).
[m]Reference 81.
[n]Reference 62.
[o]Reference 82.
[p]Reference 83.
[q]Reference 69.
[r]Reference 37; the band at 2601.13 cm^{-1} was originally assigned to $3\nu_7 + \nu_8$, which is shifted toward 2596.31 cm^{-1} upon ^{13}C substitution.[28]
[s]Reference 41.
[t]Reference 63.
[u]Reference 33.
[v]Reference 69.
[w]Reference 4.
[x]Reference 84.
[y]Reference 36.
[z]Reference 78.

DATA AVAILABILITY

The data that support the findings of this study are available within the article (and its supplementary material).

REFERENCES

[1] L. G. Bonner and R. Hofstadter, "Vibration spectra and molecular structure IV. The infra-red absorption spectra of the double and single molecules of formic acid," J. Chem. Phys. **6**, 531–534 (1938).

[2] L. G. Bonner and J. S. Kirby-Smith, "The Raman spectrum of formic acid vapor," Phys. Rev. **57**, 1078 (1940).

[3] R. L. Redington, "Vibrational spectra and normal coordinate analysis of isotopically labeled formic acid monomers," J. Mol. Spectrosc. **65**, 171–189 (1977).

[4] J. E. Bertie and K. H. Michaelian, "The Raman spectra of gaseous formic acid $-h_2$ and $-d_2$," J. Chem. Phys. **76**, 886–894 (1982).

[5] M. Pettersson, J. Lundell, L. Khriachtchev, and M. Räsänen, "IR spectrum of the other rotamer of formic acid, *cis*-HCOOH," J. Am. Chem. Soc. **119**, 11715–11716 (1997).

[6] D. Hurtmans, F. Herregodts, M. Herman, J. Liévin, A. Campargue, A. Garnache, and A. A. Kachanov, "Spectroscopic and *ab initio* investigation of the ν_{OH} overtone excitation in *trans*-formic acid," J. Chem. Phys. **113**, 1535–1545 (2000).

[7] M. Freytes, D. Hurtmans, S. Kassi, J. Liévin, J. Vander Auwera, A. Campargue, and M. Herman, "Overtone spectroscopy of formic acid," Chem. Phys. **283**, 47–61 (2002).

[8] O. I. Baskakov, I. A. Markov, E. A. Alekseev, R. A. Motiyenko, J. Lohilahti, V.-M. Horneman, B. P. Winnewisser, I. R. Medvedev, and F. C. De Lucia, "Simultaneous analysis of rovibrational and rotational data for the 4^1, 5^1, 6^1, 7^2, 8^1, 7^19^1 and 9^2 states of HCOOH," J. Mol. Struct. **795**, 54–77 (2006).

[9] A. Perrin, J. Vander Auwera, and Z. Zelinger, "High-resolution Fourier transform study of the ν_3 fundamental band of *trans*-formic acid," J. Quant. Spectrosc. Radiat. Transfer **110**, 743–755 (2009).

[10] A. Domanskaya, K. Marushkevich, L. Khriachtchev, and M. Räsänen, "Spectroscopic study of *cis*-to-*trans* tunneling reaction of HCOOD in rare gas matrices," J. Chem. Phys. **130**, 154509 (2009).

[11] K. A. E. Meyer and M. A. Suhm, "Stretching of *cis*-formic acid: Warm-up and cool-down as molecular work-out," Chem. Sci. **10**, 6285–6294 (2019).

[12] K. Hull, T. Wells, B. E. Billinghurst, H. Bunn, and P. L. Raston, "Synchrotron-based infrared spectroscopy of formic acid: Confirmation of the reassignment of Fermi-coupled 8 μm states," AIP Adv. **9**, 015021 (2019).

[13] D. Luckhaus, M. Quack, and M. Willeke, "Coupling across bonds: *Ab Initio* calculations for the anharmonic vibrational resonance dynamics of the coupled OH and CH chromophores in trans formic acid HCOOH," Z. Phys. Chem. **214**, 1087–1114 (2000).

[14] J. Demaison, M. Herman, and J. Liévin, "Anharmonic force field of *cis*- and *trans*-formic acid from high-level *ab initio* calculations, and analysis of resonance polyads," J. Chem. Phys. **126**, 164305 (2007).

[15] Y. Scribano and D. M. Benoit, "Calculation of vibrational frequencies through a variational reduced-coupling approach," J. Chem. Phys. **127**, 164118 (2007).

[16] D. P. Tew and W. Mizukami, "Ab initio vibrational spectroscopy of *cis*- and *trans*-formic acid from a global potential energy surface," J. Phys. Chem. A **120**, 9815–9828 (2016).

[17] F. Richter and P. Carbonnière, "Vibrational treatment of the formic acid double minimum case in valence coordinates," J. Chem. Phys. **148**, 064303 (2018).

[18] A. Aerts, P. Carbonnière, F. Richter, and A. Brown, "Vibrational states of deuterated *trans*- and *cis*-formic acid: DCOOH, HCOOD, and DCOOD," J. Chem. Phys. **152**, 024305 (2020).

[19] L. Nemes, A. R. W. McKellar, and J. W. C. Johns, "Laser-Stark and Fourier-transform spectroscopy of the ν_3 band of monodeuterated formic acid, HCOOD," J. Opt. Soc. Am. B **4**, 1165–1172 (1987).

[20] A. Perrin, J.-M. Flaud, B. Bakri, J. Demaison, O. Baskakov, S. V. Sirota, M. Herman, and J. Vander Auwera, "New high-resolution analysis of the ν_7 and ν_9 fundamental bands of *trans*-formic acid by Fourier transform infrared and millimeter-wave spectroscopy," J. Mol. Spectrosc. **216**, 203–213 (2002).

[21] A. Deldalle, D. Dangoisse, J. P. Splingard, and J. Bellet, "Accurate measurements of CW optically pumped FIR laser lines of formic acid molecule and its isotopic species $H^{13}COOH$, HCOOD and DCOOD," Opt. Commun. **22**, 333–336 (1977).

[22] D. Dangoisse and P. Glorieux, "Optically pumped continuous wave submillimeter emissions from $H^{13}COOH$: Measurements and assignments," J. Mol. Spectrosc. **92**, 283–297 (1982).

[23] G. M. R. S. Luiz, A. Scalabrin, and D. Pereira, "Gas phase infrared Fourier transform spectra of $H^{12}COOH$ and $H^{13}COOH$," Infrared Phys. Technol. **38**, 45–49 (1997).

[24] P. P. Ong, K. L. Goh, and H. H. Teo, "Analysis of high-resolution FTIR spectrum of the ν_6 band of $H^{13}COOH$," J. Mol. Spectrosc. **194**, 203–205 (1999).

[25] O. I. Baskakov, B. P. Winnewisser, I. R. Medvedev, and F. C. De Lucia, "The millimeter wave spectrum of *cis*-HCOOH in the ground state and in the $\nu_9 = 1$ and $\nu_7 = 1$ excited vibrational states, and *cis*-$H^{13}COOH$ in the ground state," J. Mol. Struct. **795**, 42–48 (2006).

[26] O. I. Baskakov, E. A. Alekseev, R. A. Motiyenko, J. Lohilahti, V.-M. Horneman, S. Alanko, B. P. Winnewisser, I. R. Medvedev, and F. C. De Lucia, "FTIR and millimeter wave investigation of the 7^1 and 9^1 states of formic acid HCOOH and $H^{13}COOH$," J. Mol. Spectrosc. **240**, 188–201 (2006).

[27] O. Baskakov, V.-M. Horneman, S. Alanko, and J. Lohilahti, "FTIR spectra of the ν_6 and ν_8 bands of ^{13}C formic acid molecule–assignment of FIR-laser lines," J. Mol. Spectrosc. **249**, 60–64 (2008).

[28] R. A'dawiah, T. L. Tan, and L. L. Ng, "High-resolution FTIR spectroscopy of $H^{13}COOD$: The ground state and $\nu_2 = 1$ state rovibrational constants," J. Mol. Spectrosc. **354**, 1–6 (2018).

[29] E. Willemot, D. Dangoisse, and J. Bellet, "Microwave spectrum of formic acid and its isotopic species in D, ^{13}C and ^{18}O. Study of Coriolis resonances between ν_7 and ν_9 vibrational excited states," J. Mol. Spectrosc. **73**, 96–119 (1978).

[30] R. Wellington Davis, A. G. Robiette, M. C. L. Gerry, E. Bjarnov, and G. Winnewisser, "Microwave spectra and centrifugal distortion constants of formic acid containing ^{13}C and ^{18}O: Refinement of the harmonic force field and the molecular structure," J. Mol. Spectrosc. **81**, 93–109 (1980).

[31] K. L. Goh, P. P. Ong, and T. L. Tan, "The ν_3 band of DCOOH," Spectrochim. Acta, Part A **55**, 2601–2614 (1999).

[32] O. I. Baskakov, S. Alanko, and M. Koivusaari, "The Coriolis-coupled states $\nu_6 = 1$ and $\nu_8 = 1$ of DCOOH," J. Mol. Spectrosc. **198**, 40–42 (1999).

[33] O. I. Baskakov, H. Bürger, and W. Jerzembeck, "The Coriolis-coupled states $\nu_7 = 1$ and $\nu_9 = 1$ of *trans*-HCOOD and *trans*-DCOOD," J. Mol. Spectrosc. **193**, 33–45 (1999).

[34] T. L. Tan, K. L. Goh, P. P. Ong, and H. H. Teo, "Rovibrational constants for the ν_6 and $2\nu_9$ bands of HCOOD by Fourier transform infrared spectroscopy," J. Mol. Spectrosc. **198**, 110–114 (1999).

[35] O. I. Baskakov, J. Lohilahti, and V.-M. Horneman, "High resolution analysis of the ν_7 and ν_9 bands of DCOOH," J. Mol. Spectrosc. **219**, 191–199 (2003).

[36] F. Madeja, A. Hecker, S. Ebbinghaus, and M. Havenith, "High resolution spectroscopy of the ν_3 band of DCOOD," Spectrochim. Acta, Part A **59**, 1773–1782 (2003).

[37] R. A'dawiah, T. L. Tan, and L. L. Ng, "The ν_2 band of formic acid-d_1 (HCOOD) by high-resolution FTIR spectroscopy," J. Mol. Spectrosc. **349**, 43–48 (2018).

[38] J. T. Hougen, "Coordinates, Hamiltonian, and symmetry operations for the small-amplitude vibrational problem in methyl-top internal-rotor molecules like CH_3CHO," J. Mol. Spectrosc. **181**, 287–296 (1997).

[39] S. Dalbouha and M. L. Senent, "Large amplitude vibrations of acetyl isocyanate, methyl cyanoformate, and acetyl cyanate," Phys. Chem. Chem. Phys. **21**, 3597–3605 (2019).

[40] A. Nejad, M. A. Suhm, and K. A. E. Meyer, "Increasing the weights in the molecular work-out of *cis*- and *trans*-formic acid: Extension of the vibrational database *via* deuteration," Phys. Chem. Chem. Phys. **22**, 25492–25501 (2020).

[41] J. E. Bertie, K. H. Michaelian, H. H. Eysel, and D. Hager, "The Raman–active O–H and O–D stretching vibrations and Raman spectra of gaseous formic acid–d_1 and –OD," J. Chem. Phys. **85**, 4779–4789 (1986).

[42]Z. Xue, "Raman spectroscopy of carboxylic acid and water aggregates," Ph.D. thesis, Logos Verlag Berlin, 2011.

[43]T. Forsting and M. A. Suhm, "Curry-jet SETUP," see https://doi.org/10.6084/m9.figshare.6395840.v1, 2019.

[44]K. A. E. Meyer, "Carboxylic acids under vibrational scrutiny: Experimental reference data to benchmark quantum chemical calculations," Ph.D. thesis, 2020; see http://hdl.handle.net/21.11130/00-1735-0000-0005-14BA-3.

[45]W. H. Hocking, "The other rotamer of formic acid, *cis*-HCOOH," Z. Naturforsch., A **31**, 1113–1121 (1976).

[46]K. A. E. Meyer and M. A. Suhm, "Vibrational exciton coupling in homo and hetero dimers of carboxylic acids studied by linear infrared and Raman jet spectroscopy," J. Chem. Phys. **149**, 104307 (2018).

[47]E. L. Sibert III, "Theoretical studies of vibrationally excited polyatomic molecules using canonical Van Vleck perturbation theory," J. Chem. Phys. **88**, 4378–4390 (1988).

[48]A. B. McCoy and E. L. Silbert III, "Perturbative approaches to highly excited molecular vibrations of H_2O, D_2O, and HDO," J. Chem. Phys. **92**, 1893–1901 (1990).

[49]S. V. Krasnoshchekov, E. V. Isayeva, and N. F. Stepanov, "Numerical-analytic implementation of the higher-order canonical Van Vleck perturbation theory for the interpretation of medium-sized molecule vibrational spectra," J. Phys. Chem. A **116**, 3691–3709 (2012).

[50]G. Simons, R. G. Parr, and J. M. Finlan, "New alternative to the Dunham potential for diatomic molecules," J. Chem. Phys. **59**, 3229–3234 (1973).

[51]H. M. Pickett, "Vibration–rotation interactions and the choice of rotating axes for polyatomic molecules," J. Chem. Phys. **56**, 1715–1723 (1972).

[52]E. B. Wilson, Jr., J. C. Decius, and P. C. Cross, *Molecular Vibrations: The Theory of Infrared and Raman Vibrational Spectra* (Dover Publications, Inc., New York, 1980).

[53]E. L. Sibert III, "VANVLK: An algebraic manipulation program for canonical Van Vleck perturbation theory," Comput. Phys. Commun. **51**, 149–160 (1988).

[54]C. Iung, F. Ribeiro, and E. L. Sibert III, "Comparison of perturbative and variational treatments of molecular vibrations: Application to the vibrational spectrum of HFCO up to 8000 cm^{-1}," J. Phys. Chem. A **110**, 5420–5429 (2006).

[55]M. M. Sprague, S. G. Ramesh, and E. L. Sibert III, "Combination of perturbative and variational methods for calculating molecular spectra: Calculation of the $v = 3 - 5$ CH stretch overtone spectrum of CHF_3," J. Chem. Phys. **124**, 114307 (2006).

[56]E. L. Sibert III and J. Castillo-Chará, "Theoretical studies of the potential surface and vibrational spectroscopy of CH_3OH and its deuterated analogs," J. Chem. Phys. **122**, 194306 (2005).

[57]H. H. Nielsen, "The vibration-rotation energies of molecules," Rev. Mod. Phys. **23**, 90–136 (1951).

[58]A. M. Rosnik and W. F. Polik, "VPT2+K spectroscopic constants and matrix elements of the transformed vibrational Hamiltonian of a polyatomic molecule with resonances using Van Vleck perturbation theory," Mol. Phys. **112**, 261–300 (2014).

[59]H.-R. Dübal and M. Quack, "Vibrational overtone spectra and vibrational dynamics of $CFHCl_2$ and $(CH_3)_2CFH$," Mol. Phys. **53**, 257–264 (1984).

[60]O. I. Baskakov and J. Demaison, "Spectroscopic study of the $\nu_6 = 1$ and $\nu_8 = 1$ vibrational states of formic acid, HCOOH: New assignments of laser transitions," J. Mol. Spectrosc. **211**, 262–272 (2002).

[61]K. G. Goroya, Y. Zhu, P. Sun, and C. Duan, "High resolution jet-cooled infrared absorption spectra of the formic acid dimer: A reinvestigation of the C–O stretch region," J. Chem. Phys. **140**, 164311 (2014).

[62]W. Luo, Y. Zhang, W. Li, and C. Duan, "Jet-cooled infrared absorption spectrum of the ν_4 fundamental band of HCOOH and HCOOD," J. Mol. Spectrosc. **334**, 22–25 (2017).

[63]S. Oswald, E. Meyer, and M. A. Suhm, "Dinitrogen as a sensor for metastable carboxylic acid dimers and a weak hydrogen bond benchmarking tool," J. Phys. Chem. A **122**, 2933–2946 (2018).

[64]D. L. Howard and H. G. Kjaergaard, "Resonance coupling in the fourth OH-stretching overtone spectrum of formic acid," J. Chem. Phys. **121**, 136–140 (2004).

[65]In the usual Placzek approximation of the polarizability and linearly polarized incident radiation, the depolarization ratio of totally symmetric bands is below a limiting value whose figure depends on the geometry of the setup (3/4 or 6/7). For the setup used in this work this is discussed in a previous publication.[85] Since the depolarization ratio of non-totally symmetric vibrations equals this limiting value they are called 'completely depolarized'. When changing the incident laser polarization relative to the scattering plane from perpendicular to parallel, the relative intensity-decrease is a measure of the degree of polarization of this band. The smaller the depolarization ratio the higher the decrease in intensity.

[66]G. Placzek, "Rayleigh-Streuung und Raman-Effekt," in *Handbuch der Radiologie*, edited by E. Marx (Akademische Verlagsgesellschaft, Leipzig, 1934), Vol. 6, pp. 205–374.

[67]D. A. Long, *The Raman Effect: A Unified Treatment of the Theory of Raman Scattering by Molecules* (Wiley, Chichester and New York, 2002).

[68]H.-R. Dübal and M. Quack, "Tridiagonal Fermi resonance structure in the IR spectrum of the excited CH chromophore in CF_3H," J. Chem. Phys. **81**, 3779–3791 (1984).

[69]V. Z. Williams, "Infra-red spectra of monomeric formic acid and its deuterated forms. II. Low frequency region (2200 − 800 cm^{-1})," J. Chem. Phys. **15**, 243–251 (1947).

[70]K. Marushkevich, L. Khriachtchev, J. Lundell, A. V. Domanskaya, and M. Räsänen, "Vibrational spectroscopy of *trans* and *cis* deuterated formic acid (HCOOD): Anharmonic calculations and experiments in argon and neon matrices," J. Mol. Spectrosc. **259**, 105–110 (2010).

[71]T. L. Tan, K. L. Goh, P. P. Ong, and H. H. Teo, "Rovibrational analysis of ν_2 and $2\nu_5$ bands of DCOOH by high resolution FTIR spectroscopy," J. Mol. Spectrosc. **198**, 387–392 (1999).

[72]A. Perrin, C. P. Rinsland, and A. Goldman, "Spectral parameters for the ν_6 region of HCOOH and its measurement in the infrared tropospheric spectrum," J. Geophys. Res.: Atmos. **104**, 18661–18666, https://doi.org/10.1029/1999jd900358 (1999).

[73]F. Madeja, P. Markwick, M. Havenith, K. Nauta, and R. E. Miller, "Rotationally resolved infrared spectroscopy of h_2- and d_1-formic acid monomer in liquid He droplets," J. Chem. Phys. **116**, 2870–2878 (2002).

[74]K. A. E. Meyer, J. A. Davies, and A. M. Ellis, "Shifting formic acid dimers into perspective: Vibrational scrutiny in helium nanodroplets," Phys. Chem. Chem. Phys. **22**, 9637–9646 (2020).

[75]S. Erfort, M. Tschöpe, G. Rauhut, X. Zeng, and D. P. Tew, "*Ab initio* calculation of rovibrational states for non-degenerate double-well potentials: *cis-trans* isomerization of HOPO," J. Chem. Phys. **152**, 174306 (2020).

[76]F. Ito and T. Nakanaga, "Jet-cooled infrared spectra of the formic acid dimer by cavity ring-down spectroscopy: Observation of the O−H stretching region," Chem. Phys. **277**, 163–169 (2002).

[77]C. Emmeluth, M. A. Suhm, and D. Luckhaus, "A monomers-in-dimers model for carboxylic acid dimers," J. Chem. Phys. **118**, 2242–2255 (2003).

[78]K. L. Goh, P. P. Ong, H. H. Teo, and T. L. Tan, "High resolution FTIR spectrum of the ν_1 band of DCOOD," Spectrochim. Acta, Part A **56**, 991–1001 (2000).

[79]R. A. Mata and M. A. Suhm, "Benchmarking quantum chemical methods: Are we heading in the right direction?" Angew. Chem., Int. Ed. **56**, 11011–11018 (2017).

[80]K. L. Goh, P. P. Ong, T. L. Tan, W. F. Wang, and H. H. Teo, "The high-resolution infrared spectrum of the ν_5 band of deuterated formic acid (DCOOH)," J. Mol. Spectrosc. **190**, 125–129 (1998).

[81]O. I. Baskakov, "The vibrational state $\nu_5 = 1$ of HCOOD," J. Mol. Spectrosc. **208**, 194–196 (2001).

[82]O. I. Baskakov, "FTIR spectrum of the ν_3 band of HCOOD," J. Mol. Spectrosc. **213**, 1–7 (2002).

[83]K. L. Goh, P. P. Ong, H. H. Teo, and T. L. Tan, "Improved rovibrational constants for the ν_3 infrared band of HCOOD," J. Mol. Spectrosc. **197**, 322–323 (1999).

[84]T. L. Tan, K. L. Goh, P. P. Ong, and H. H. Teo, "FTIR spectrum of the ν_4 band of DCOOD," J. Mol. Spectrosc. **195**, 324–327 (1999).

[85]M. Gawrilow and M. A. Suhm, "2-methoxyethanol: Harmonic tricks, anharmonic challenges and chirality-sensitive chain aggregation," Phys. Chem. Chem. Phys. **22**, 15303–15311 (2020).